RAPID SYNTHESIS OF DUAL-LAYERED COVALENT ORGANIC FRAMEWORK MEMBRANES VIA INTERFACIAL POLYMERIZATION WITH ENHANCED DESALINATION PERFORMANCE

by

Miguel Angel Jaimes

A Thesis Submitted in

Partial Fulfillment of the

Requirements for the Degree of

Master of Science

in Engineering

at

The University of Wisconsin-Milwaukee

May 2023

ABSTRACT

RAPID SYNTHESIS OF DUAL-LAYERED COVALENT ORGANIC FRAMEWORK MEMBRANES VIA INTERFACIAL POLYMERIZATION WITH ENHANCED DESALINATION PERFORMANCE

by

Miguel Angel Jaimes

The University of Wisconsin-Milwaukee, 2023
Under the Supervision of Professor Xiaoli Ma

As a consequence of disrupting the water cycle via human interventions, such as climate change, humanity is facing global water crises. The water crises are wide ranging, but often associated with the deterioration of a local water cycle's capacity to support a population. This capacity is reduced on a global scale through the atmosphere via climate change, but on a local scale, it can be reduced because of an over extraction of resources, alteration of ecosystems, and water pollution.

The deployment of desalination plants is growing around the world. Reverse osmosis (RO) desalination is much more efficient than the thermal processes that came before it, such as distillation. However, RO desalination plants are large and still consume commensurate amounts of energy. By increasing the efficiency of potable water production, capital costs for implementation of RO solutions become more viable.

The reliability and efficiency of membrane separation will be affected by the materials the membrane is made of. Generally, all membranes exhibit a behavior that is known as the tradeoff between selectivity and permeability. Membranes with high selectivity will have a low

permeability/permeance and vice versa. Covalent Organic Framework materials as membranes may have the potential to exceed the current performance limits of state-of-the-art RO thin film composite (TFC) membranes.

COF materials are 2D or 3D networks with intrinsic microporosity that are made with geometric linker molecules. The goal of this study is to enhance the desalination performance of COF membranes. The objective of this study was to utilize rapid interfacial polymerization to produce dual-layered COF membranes to enhance desalination. The hypothesis was that the presence of a second layer would increase rejection. This question has been studied with long reaction times, but never with rapid synthesis. The performance of the membranes was tested by measuring water permeances and the rejection rates of salts. The membranes were able to remove salts from the water, and the characterization of the membranes showed that the introduction of a second layer shifted the pore size distribution to smaller mean pore sizes in the COF membranes which led to improved salt rejection.

I want to dedicate this to the women in my family who have taught me the most important lessons in life. My mother, Imelda. My sisters, Joanna, Emily, and Brittany. And to my beloved wife, Daniela.

Also, in loving memory of the best orange cat to ever exist, Nagato.

Who brought me sunrise at 3AM.

TABLE OF CONTENTS

LIST OF FIGURES

LIST OF ABBREVIATIONS

RO	Reverse Osmosis
COF	Covalent Organic Framework
TFC	Thin Film Composite
NF	Nanofiltration
SWRO	Sea Water Reverse Osmosis
MSF	Multi-Stage Flash Desalination
MED	Multi-Effect Desalination
GRACE	Gravity Recovery and Climate Experiment
MF	Micro Filtration
UF	Ultra Filtration
PFTE	Polytetrafluoroethylene
PES	Polyether Sulfone
Tp	2,4,6-trihydroxybenzene-1,3,5-tricarbaldehyde
Pa1	p-phenylene diamine
Pa2	2,5-dimethyl-1,4-phenylenediamine
$PaNO_2$	2-nitro-1,4-phenylenediamine
$Pa(OH)_2$	2,5-diaminohydroquinone dihydrochloride
Hz	Hydrazine monohydrate
TpPa1	Single Layer COF membrane made from Tp and Pa1

TpPa2	Single Layer COF membrane made from Tp and Pa2
$TpPaNO_2$	Single Layer COF membrane made from Tp and $PaNO_2$
$TpPa(OH)_2$	Single Layer COF membrane made from Tp and $Pa(OH)_2$
TpHz	Single Layer COF membrane made from Tp and Hz
TpPa1 TpPa2	Dual Layer COF membrane made from TpPa1 TpPa2
TpPa1 TpHz	Dual Layer COF membrane made from TpPa1 TpHz
$TpPaNO_2$ TpHz	Dual Layer COF membrane made from $TpPaNO_2$ TpHz
NaCl	Sodium sulfate
$MgSO_4$	Magnesium sulfate
Na_2SO_4	Sodium sulfate

ACKNOWLEDGEMENTS

I am deeply grateful to my professor, Dr. Xiaoli Ma, for his unwavering support and guidance throughout my time in the program. He provided me with a great deal of independence and room to grow as a scientist. Their encouragement and belief in my abilities have been invaluable, especially during the challenging times of the Covid 19 pandemic when it was difficult to be in the lab.

I would also like to extend my heartfelt thanks to my lab mates for their hard work, dedication, and support throughout my research journey. They have made every day in the lab a bright and enjoyable one, and I could not have completed important characterizations without their help. Their friendship and the discussions we had about a smorgasbord of issues have also been greatly appreciated. I am grateful for the opportunity to work with such a talented and dedicated group of individuals. In addition, I would like to thank Chris Ney, Rob, Tim, Randy, and Mark. Your contributions have been invaluable and greatly appreciated. I am thankful for the support and resources provided by School of Freshwater Sciences. I am also grateful for the Advanced Opportunity Program which allowed me to focus on my research and achieve my goals. I would also like to thank any other individuals or organizations that provided support or assistance for their help and guidance.

Finally, I would like to express my gratitude to my family and friends for their love and support throughout my academic journey. Their encouragement and belief in me have meant the world to me, and I could not have done it without them. Thank you for always being there for me.

Chapter 1: Introduction

Research Motivation

Global Water Crisis

In order for a living organism to survive, it needs to have water. Therefore, survival is dependent on an organism's ability to integrate itself into the water cycle. Plants tap into the water cycle through their roots. Animals tap into the water cycle by drinking water from rivers, lakes, and ponds. Humans have disrupted all aspects of the water cycle by polluting water sources, over-extracting water from rivers and aquafers, altering landscapes through activities such as deforestation, urbanization, and dam construction.[1] Climate change then leads to changes in precipitation patterns, increased flooding, and droughts.[1,25]

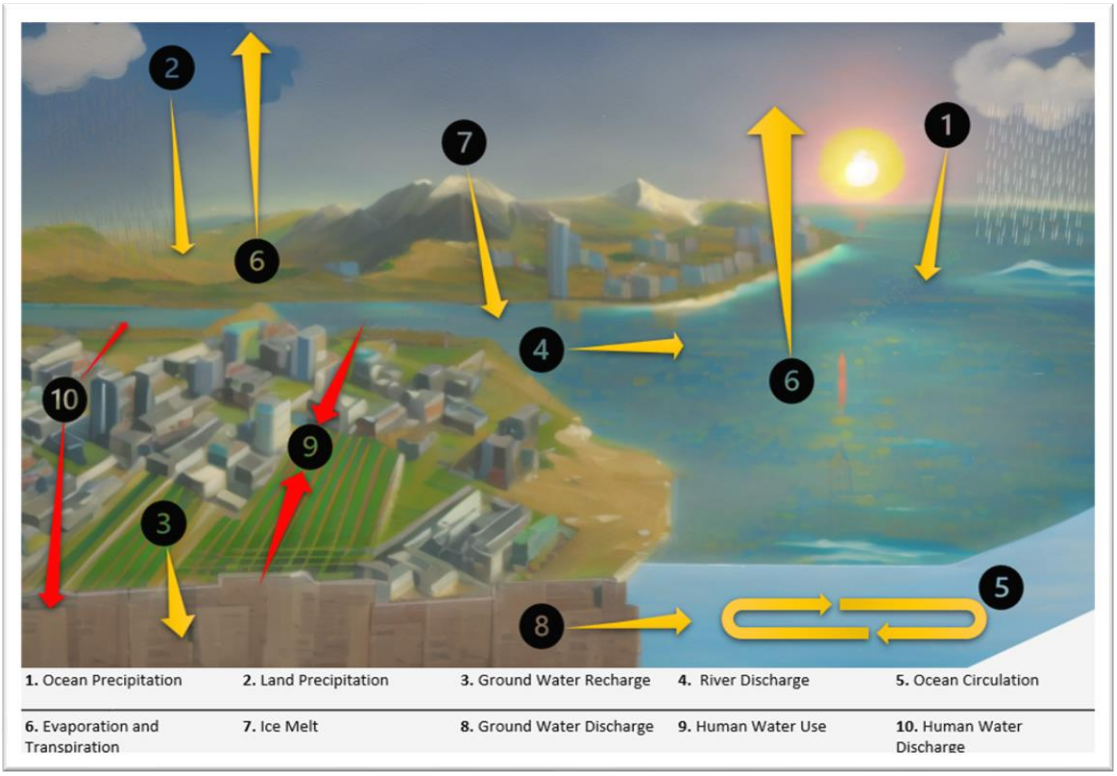

Figure 1: A simple illustration of a water cycle with human influences. Human influences are highlighted with red arrows.

According to the latest IPCC report, at least half of the worlds current population will experience severe water scarcity for at least one month out of the year.[25] Every degree of global warming will increase drought flooding and harm to society, exacerbating water related issues.[25] In Figure 3, it can be seen that many parts of the world are already at high risk of drought. Solutions that reduce carbon emissions and promote efficient use of water will be appropriate to achieve water security sustainably.[25]

Modern human activity requires a lot of water. At a global level, most water is produced in order to power industry, agriculture, generate electricity, and as a source of potable water for the public.[26] Looking at figure 2, it can be seen that global water use is stratified. Poor and arid nations are often using less water. And finally, to understand how local water supplies are changing, figure 4, a global map colored by the average net gain or loss of some volume of water over the course of a year, shows that there are many areas that are losing water on a yearly basis. The map is based on data from the Gravity Recovery and Climate Experiment (GRACE) satellite mission, which measures changes in the Earth's gravity field caused by changes in the distribution of mass, including water. The map shows areas of the Earth where there has been a net gain or loss of water over the course of a year, highlighting regions that are experiencing changes in water availability. The figure also includes information about the potential causes of water flux in select regions, indicating whether it is likely caused by climate change, direct human impact, or natural variability. Understanding the global water flux and its potential causes is important for managing water resources and addressing issues related to water availability and sustainability. When comparing the water stressed regions, to areas that are losing water, we can understand how it is possible that by the year 2050, that half of the world’s population is going to be living in water stressed regions of the world.[25]

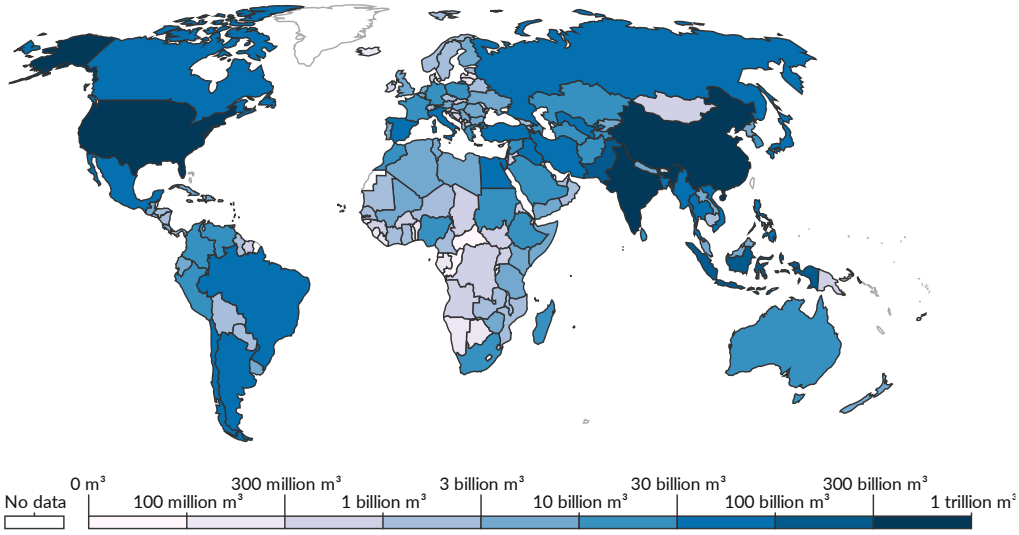

Figure 2: 2017 fresh water withdraws from agriculture, industry, and municipal sectors. a global map with each country colored according to the amount of water it withdrew in 2017. The map provides a visual representation of the distribution of water use around the world. (Ritchie, H., Roser, M.)

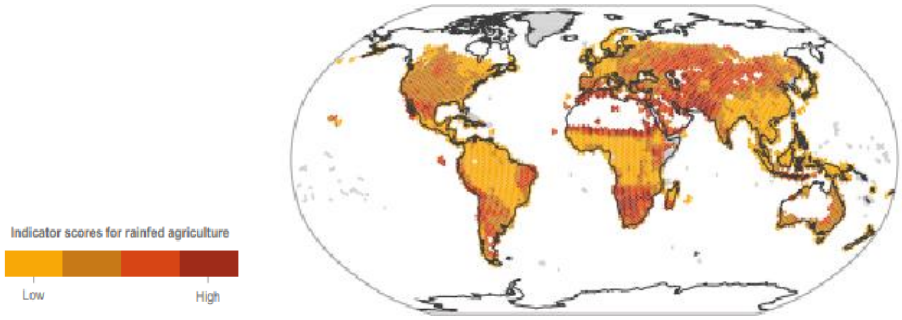

Figure 3: Drought Risk Indication for Rain Fed Agriculture. A global map of the regions that are of high risk for drought. (IPCC, Meza et al.)

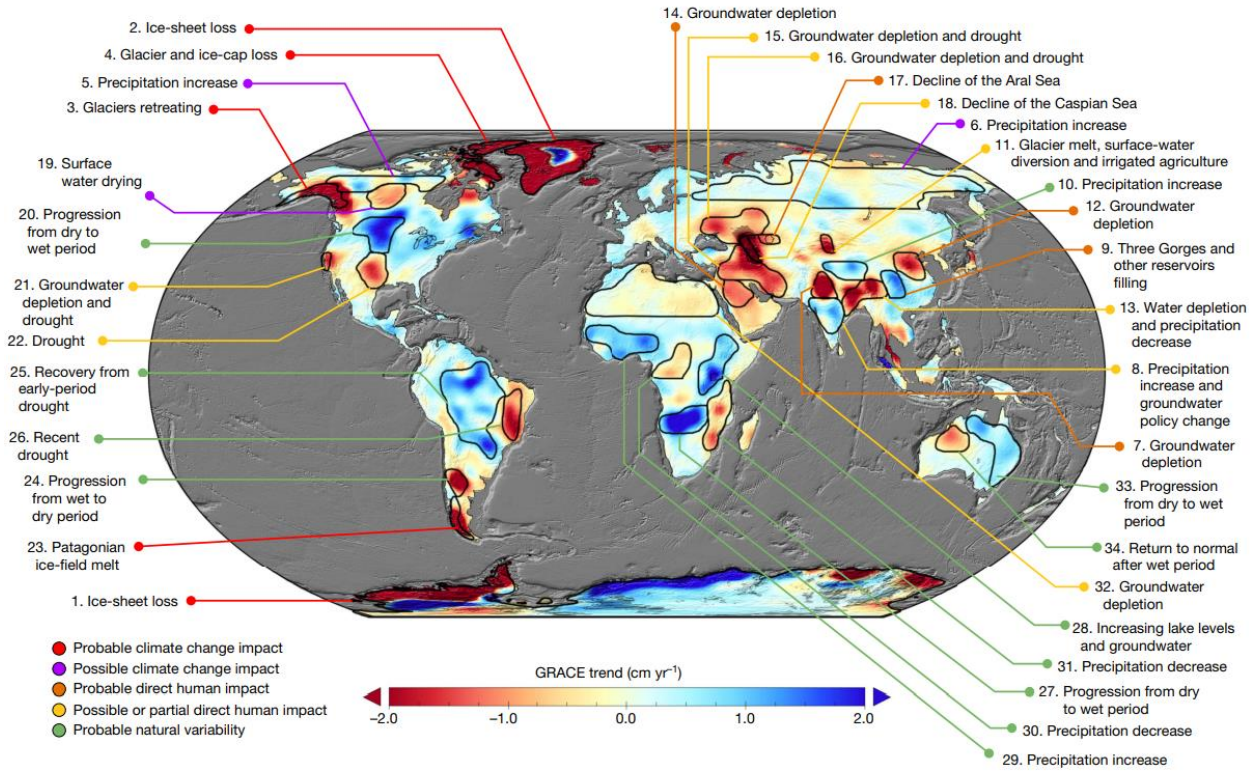

Figure 4: Global Water Flux and Causes: Global map showing average annual water flux from GRACE satellite data, highlighting regions experiencing changes in water availability and potential causes (climate change, human impact, natural variability). (Rodell et al.)

Understandably, water production continues to be a global challenge in the face of looming water crises. In 2017, 5 billion people utilized safe drinking water services, 1.4 billion used basic water services, 435 million people used unimproved water sources, 144 million people were utilizing surface waters, and 785 million people had no access to basic water services.[12] Water scarcity is a real threat to large populations across the globe. And while desalination may not be the best option for every situation, desalination of brackish and or seawater has worked to supplement or completely replace the water supply in some countries.

Water Scarcity

At first glance, global water crises sound paradoxical given that water is not uncommon compound on Earth. Water is abundant, but surprisingly little of it is accessible or fit for consumption.

Speaking of inaccessible, all ocean water is too salty to consume, 0.2 to 2 oceans worth of water are estimated to be locked away in the Earth's mantle[23], most fresh water is locked up in polar glaciers, so that leaves underground aquifers and surface water as the most accessible sources of drinking water. Unfortunately, aquifers are dependent on rainfall to sustain their levels, and surface water management is becoming a challenge in some areas use.[10,14] Additionally, recent reports from the IPCC and data from NASA's GRACE mission confirm the idea that wet regions are getting wetter and dry regions are getting drier.[25,26]

Desalination

Desalination membranes are used in state-of-the-art desalination plants around the world where they make sense. Understandably, the deployment of desalination plants is not strongly correlated with water scarcity. The deployment of desalination plants is more likely to emerge when favorable conditions, potential to drive economic growth, political, and investment opportunity align[36] There are many policy and cultural factors that are a play that can help bring about more use of membrane desalination plants, but as material scientist, we are in a unique spot where we are able to increase the efficiency of a process. By making the technology much more effective and economical, the development of new desalination plants will be accelerated.

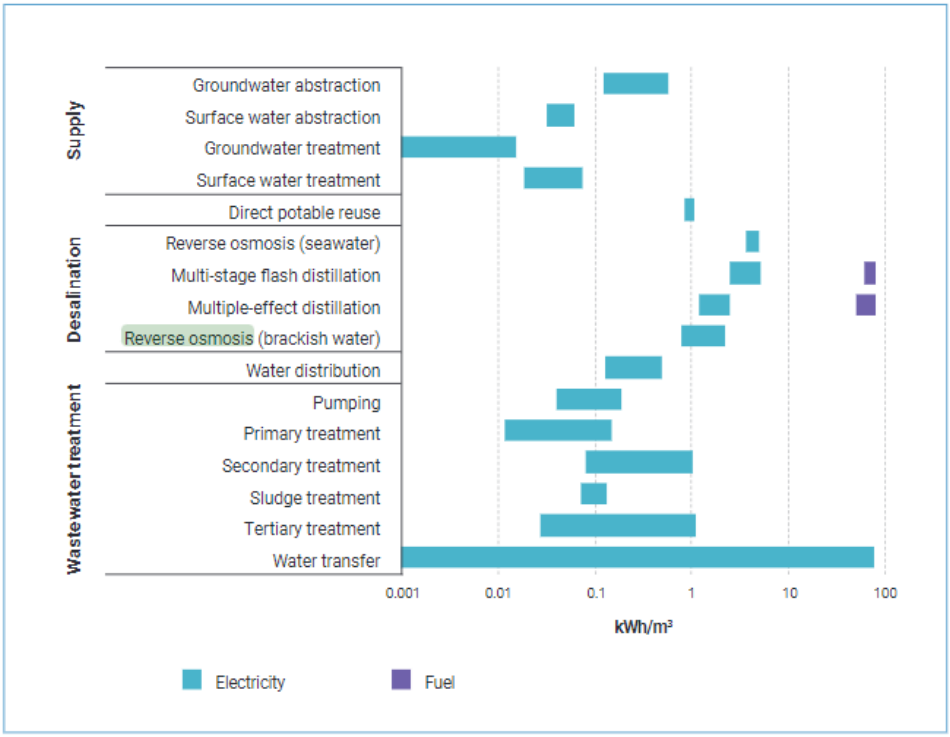

Figure 5: displays the energy use for different processes in the water sector, in terms of kilowatt-hours per cubic meter of water produced. (IEA 2016a)

Background of Desalination

Desalination is the process of converting saltwater into freshwater by removing salts and other minerals from it. Desalination technology has been around since the 1800s but has advanced greatly over the years with the development of new membrane materials and process optimization. Figure 5 highlights that different processes have different energy demands and that of desalination processes, RO has the lowest energy consumption. The current focus is on making the technology more efficient and accessible so that it can be used to provide fresh water to regions suffering from water shortages. Research is being conducted into renewable energy sources and better membrane materials to reduce the cost of desalination, as well as new pre-treatment methods to reduce fouling in membrane systems. Ultimately, these advances will make desalination technology more accessible and less energy-intensive,

providing a reliable source of clean water for regions in need. Mainstream proponents of desalination technology are hoping that the technology will be more widely adopted in the future to address global water scarcity issues.

To desalt water at large scales, thermal desalination processes such as, multi-stage flash distillation plants (MSF) and multi-effect desalination plants (MED) were originally used, but since the 1950s, seawater reverse osmosis plants (SWRO) have become the dominant technology due to their lower energy requirements.[8,36] In 2012, thermal processes produced 34.2% of the world's total desalination capacity, but this number decreased to 24% by 2020 as SWRO increased from 63.7% to 69%. Reverse osmosis is preferred over thermal desalination due to its energy and cost efficiency.[4] In the early 2000s, several technological advances were made in SWRO desalination, including developing improved membranes that reduce fouling and using energy recovery devices that reduce the energy required for desalination.

Membrane Desalination

The first membrane and the first observation of osmosis was discovered in 1748.[4] Eventually, in the 1950s the first commercially viable high-pressure RO system was create. Since then, improvements in membrane materials have been made, enabling the development of higher-flux membranes, and leading to a new wave of RO desalination systems. The practicality of desalination technology has improved in the 2000s by using renewables, such as solar and wind, to power desalination plants. Desalination is becoming increasingly important in regions suffering from water shortages due to overpopulation, climate change, and other factors.

Membrane desalination is very energy efficient. In fact, current desalination plants are operating near thermodynamic limits.[2,5,24,35] This limits the further development of desalination processes with newer membranes and other developments. To increase the efficiency of membrane desalination and

reduce energy consumption, researchers are focusing on developing better membranes, optimizing the design of membrane-based systems, improving RO process control, and developing more efficient energy recovery systems.[2,8,35]

By 2020, more than 17,000 desalination plants had been built globally, with a total desalination capacity of over 86 million cubic meter per day.[36] As the global demand for clean water continues to increase, the need for desalination technology will also rise.

It is evident that there is a significant disparity when it comes to the deployment of desalination technology. Investment in further research into sustainable materials for desalination plants is needed in order to bring water independence to people living in water-scarce regions. Membranes and other materials that are able to reduce fouling and increase the efficiency of desalination processes could be immensely beneficial in making desalination both more cost-effective and accessible. By doing so, the disparities in water supply could be alleviated and even the most water-stressed areas could have access to an ample and safe source of drinking water.

RO is the dominant technology in deployed desalination. As shown in figure 6, the growth of global desalination capacity over time, broken down by the share of each desalination technology. There are several different technologies Figure 7, that can be used for desalination, including RO, thermal processes, and electrodialysis. The figure shows the growth of global desalination capacity year by year, highlighting the share of each technology. The data illustrates that RO is the dominant technology for desalination, with a consistently high share of the global capacity. There are no signs that RO membrane technology will be challenged by non-membrane-based desalination in the near future. The technology is mature. Membrane materials that are compatible with the current supply chain and manufacture of RO membranes will have a better chance of deployment. There is a need for new membrane materials that can be used to increase desalination efficiency, reduce desalination footprint, capital cost, and

environmental concerns.

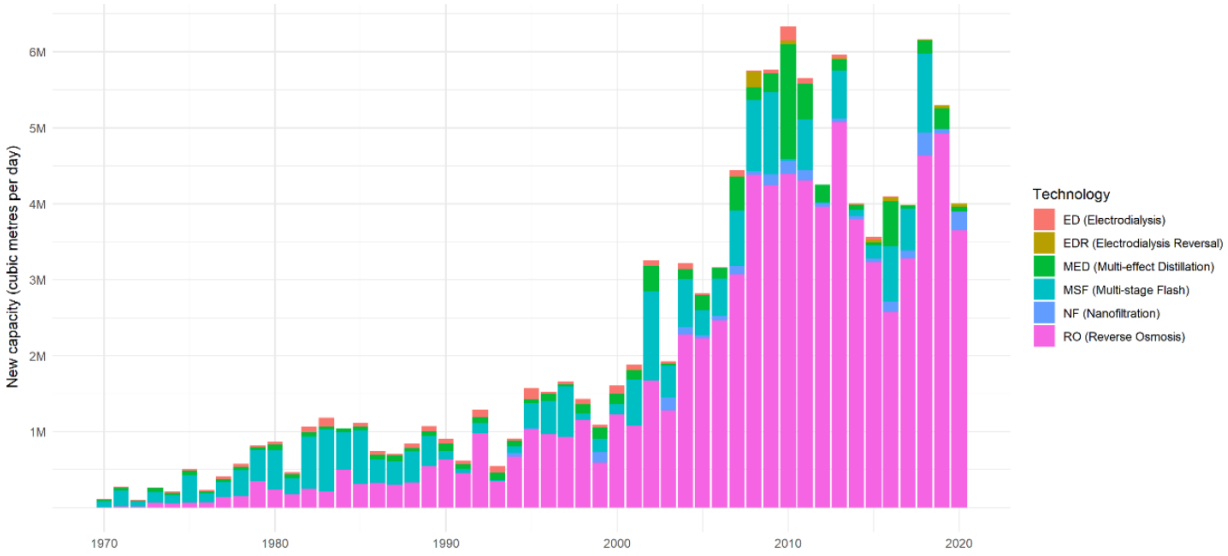

Figure 6: Global Desalination Capacity by Technology: illustrates the growth of global desalination capacity over time, broken down by the share of each technology, with reverse osmosis being the dominant technology. (Williams, J.)

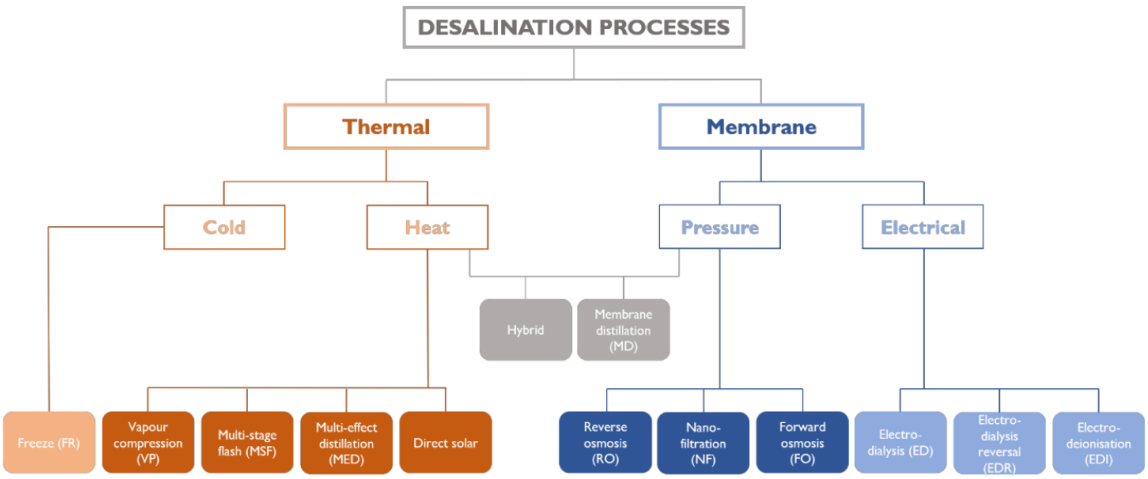

Figure 7: Desalination Methods and Technologies: illustrates the different methods of desalination using a tree, split into thermal and membrane processes, highlighting the diversity of technologies available for desalination and their unique characteristics and capabilities. (Williams, J.)

NF & RO limitations

Thin film composite (TFC) membranes, such as polyamide NF and RO membranes have become dominant in desalination due to their exceptional salt rejection and efficiency.[2,24] This performance can be attributed to the use of polyamide as the primary material comprising the selective layer in most modern TFC membranes. Through incremental increases in permeability/permeance (permeance is equal to permeability normalized by membrane thickness) and rejection, this technology is slowly increasing the efficiency of desalination. Despite ongoing efforts to improve the performance of polyamide-based membranes, they still require pre-treatment and post-treatment to achieve optimal desalination results. To further enhance the performance of TFC membranes, research and development efforts are focused on the development of new membrane materials that have higher rejection, higher permeance, or both.[2,24,35] Higher rejection would decrease the amount of post treatment needed, and higher permeance could lower the specific energy required to produce adequate clean water. In addition to this, new materials may help minimize the need for pre-treatment by reducing the risk of damage or fouling.

Nanoporous COF membranes could offer advantages over traditional NF and RO membranes such as higher water permeance, greater, controllable, and more precise selectivity for targeted ions, lower fouling rates, and improved chemical stability in harsh environments. These characteristics make COF membranes a potential alternative for certain desalination applications where traditional methods may not be suitable.

Membrane Separation

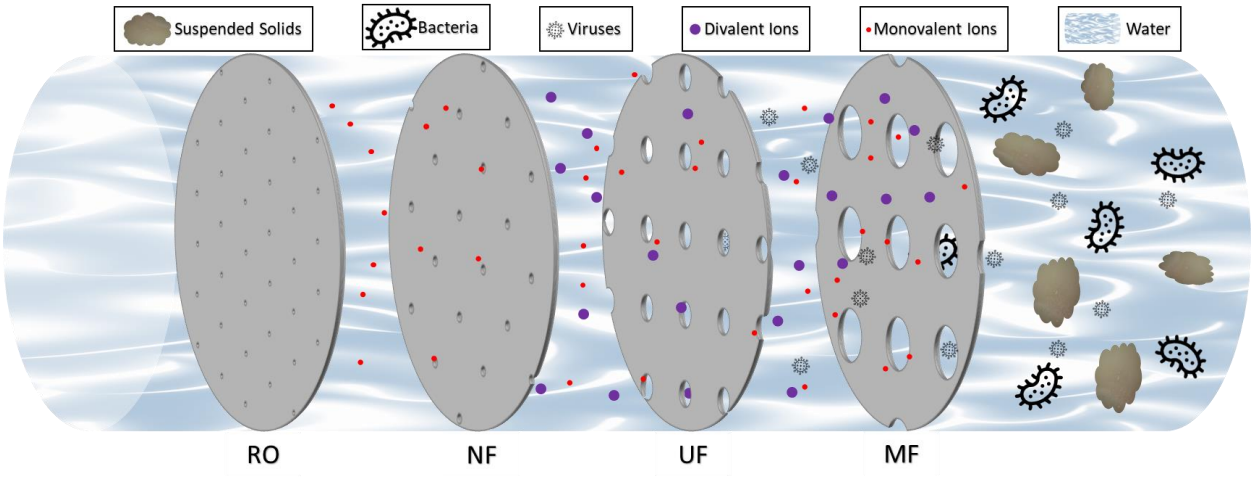

Figure 8: An illustration of the range of rejection by different membrane filtration types. Microfiltration (MF) pore size range from 0.1 to 10 micrometers. Ultrafiltration (UF) pore size range of 10 to 100 nanometers. Nanofiltration (NF) pore size range from 1 to 10 nanometers. Reverse osmosis membranes pore size range of less than 1 nanometer.

Filtration is a process used to separate particles and impurities from a fluid. There are different types of filtrations, each with its own set of characteristics and applications. Microfiltration (MF) is used to remove particles larger than 0.1 microns in size. It is typically used in pre-treatment stages of filtration processes to remove large particles before subjecting the fluid to further treatment. Ultrafiltration (UF) has smaller pore sizes, ranging between 0.01-0.1 microns, it can remove smaller particles such as bacteria or viruses while allowing water molecules to pass through. RO uses hydraulic pressure higher than osmotic pressure to force saltwater through a membrane, leaving behind pure water on one side and a concentrated brine solution on the other side. This method is highly efficient in removing dissolved salts and other impurities from water. Figure 8 illustrates the different size range for filtration.

Membrane Materials

Nanoporous Membrane Materials

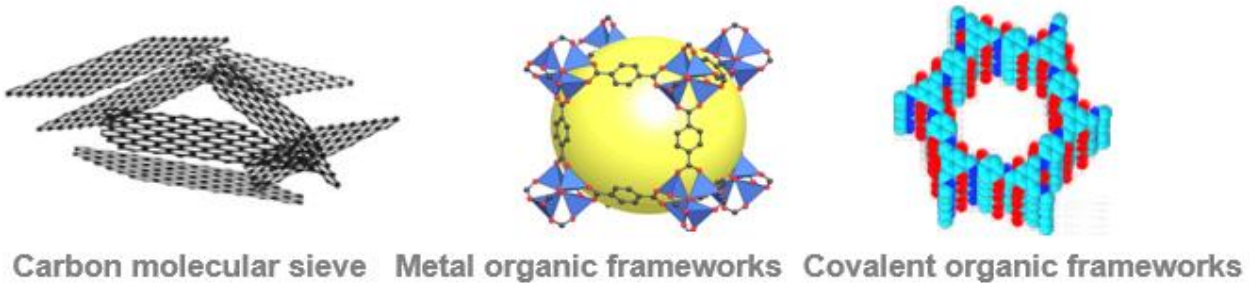

Figure 9: Nanoporous membrane materials: illustrates several nanoporous membrane materials.

Figure 9 illustrates several nanoporous membrane materials that can be used for a variety of filtration and separation applications. From left to right, the materials shown include carbon molecular sieves, metal-organic frameworks, and COFs. These materials have pore sizes on the nanometer scale, typically less than 2 nm, which makes them suitable for use in applications where smaller particles or molecules need to be separated or filtered. The bottom-up synthesis of these materials can be used to tailor their separation properties, enabling the precise control of pore size, shape and functionality of the membrane.

COF Materials

COFs are an emerging class of porous materials. COFs exhibit regular 2D or 3D ordered structure. They possess properties including crystallinity, inherent ordered 2D or 3D pore structure, tunable pore size, a high capacity for functionalization, and excellent thermal and chemical stability. Figure 10 demonstrates how molecular building blocks come together to form an ordered structure. This makes them suitable for a wide range of practical applications. Reticular chemistry (new branch of chemistry that describes framework structures like COFs) has fueled interest in COFs and as a result, numerous studies have shown that COFs have promise for use in gas storage, catalysts, membranes, drug delivery, energy storage, and more.[15,16,21,39]

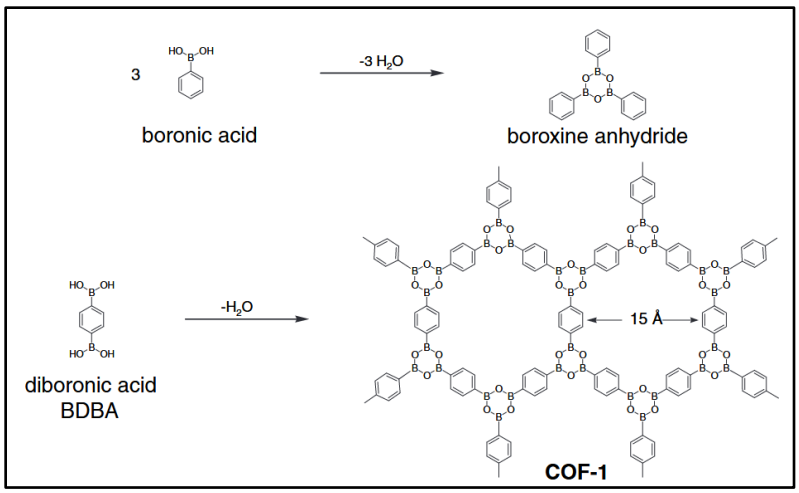

Figure 10: figure illustrates a covalent organic framework, COF-1 built from a molecular building block to produce a porous material with high surface area and tunable pore size. (Cote et al.)

β-ketoenamine COFs

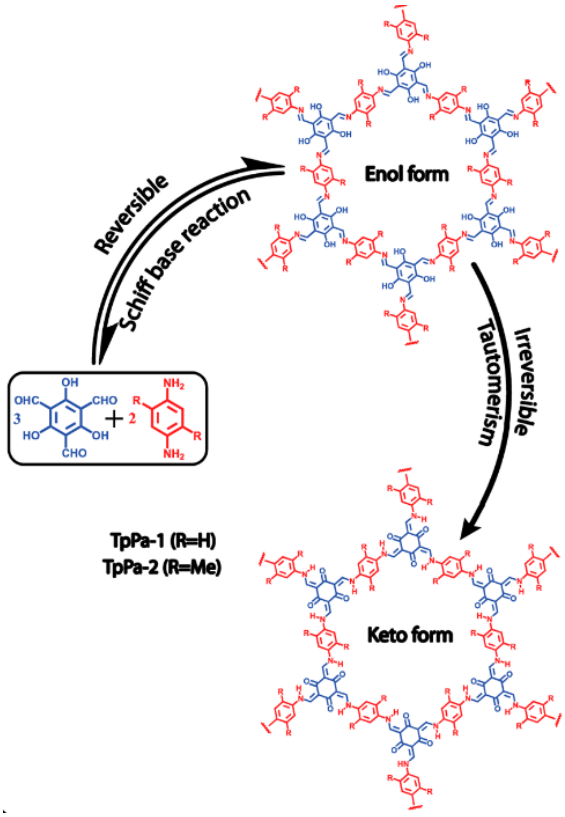

Figure 11: The synthesis of beta-ketoenamine COFs through the formation of imine bonds, followed by the irreversible tautomerism of the COF to its ketoenamine form. (Kandambeth et al)

The materials used in this study were TpPa1, TpPa2, $TpPaNO_2$, $TpPa(OH)_2$ and TpHz. These

membranes are all a part of the COF family that exhibit beta-enamine linkages, which make them exceptionally stable.[16] They first link together via imine bonding which is reversible. A Schiff base reaction involves the condensation of an aldehyde (a molecule containing a carbonyl group) with a primary amine (a molecule containing an amine group) to form a linkage which have enol and imine moieties. This process is outlined in figure 11. This reaction typically occurs in an acidic solution, where the aldehyde and amine react to form a new compound called a Schiff base. In the reaction, the carbonyl group of the aldehyde reacts with the amine group of the primary amine to form an imine bond. Schiff-base reactions are reversible. The reversible Schiff-base reaction is typically catalyzed by an acid. In the presence of an acid, the reaction proceeds in the forward direction, forming the Schiff base from the aldehyde and amine. When the COF monomers begin to react, they will most likely form the kinetic, amorphous product. The reversibility of these Schiff base reactions, error correction of the lattice via the formation of new bonds and the breaking of old bonds, is essential for the creation of a crystalline structure with a highly ordered arrangement of molecules. These COFs then undergo a second irreversible reaction step, enol-keto tautomerization. Enol-keto tautomerization is a chemical reaction in which a molecule containing an enol group (an alcohol group and double bonded carbon atoms) is converted to the keto form (compound containing a carbonyl group, where a carbon atom is double bonded to an oxygen atom). In these COFs the irreversible tautomerization refers to the enol → keto, imine → enamine tautomerizations. Tautomerization is a type of structural isomerism in which a molecule can exist in two or more forms that have the same atoms, but different arrangements of chemical bonds. These COF linkages are commonly referred to as beta keto-enamine linkages.

COF Membranes

The synthesis of COFs has progressed from solvothermal synthesis to room temperature synthesis and the development of self-standing thin films, and more recently, the synthesis of COFs directly onto porous substrates.

Solvothermal synthesis of COFs involves the use of high temperatures and aggressive solvents, to condense organic monomers into the desired COF structure. This method produces COFs as insoluble, microcrystalline powders, but the use of aggressive solvents and high temperatures can be challenging and can limit the morphology of the end product. Such conditions are not amenable for the formation of TFC membranes on polymeric substrates.

To address these limitations, researchers have developed methods for synthesizing COFs at room temperature using milder solvents. This approach allows for the use of a wider range of polymeric materials, but the resulting COFs are still often produced as thick, uniform films that lack an asymmetric structure and are not suitable for small organic molecules.

To overcome these limitations, researchers have focused on developing methods for synthesizing thin, self-standing COF films. One approach involves using interfacial polymerization (IP) reactions to produce thin COF films on a water/organic interface. These films can be transferred to porous substrates to form composite membranes, but the process can be complex and time-consuming, and the adhesion of the COFs to the substrates can be an issue. More recently, researchers have explored the direct synthesis of COFs onto porous substrates, using monomer pairs that react to achieve growth of COFs within a short period of time. This approach allows for the production of high performing membranes that outperform those prepared by other methods and has the potential for scaling up for real-world applications.[3,21]

COF Membranes for Desalination

Research in COF membranes has grown, but most COF membranes in the literature focus on molecular separations rather than desalination. Although theoretically COF materials hold great promise for highly efficient desalination membranes. [3,30,31]

COF Membrane Simulations

Molecular dynamics of monolithic TpPa-X COF 2D sheets has shown high water permeance 3 orders of magnitude higher than conventional RO membranes, and high desalination performance up to 99.4%.[43] Since the first synthesis of 2D COFs, it was hypothesized that there could be different stacking modes of COFs.[6] In the context of COF membranes, this provides researchers with an avenue to increase the rejection of membranes. One simulation showed that rejection in TpPa1 membranes does increase when the layers are offset.[46]

Pure COF Active Layer

As mentioned earlier, TFC membranes that utilize pure COF as the selective layer do not have a large presence in the literature as desalination membranes, although there are notable exceptions. The following papers focus on the synthesis methods that improve the desalination performance of COF TFCs. Wang et al. demonstrated the secondary growth of COF using counter diffusion of the monomers. The layers were made using unidirectional diffusion synthesis. The first layer was synthesized over a period of 6 hours. Then the secondary growth step occurred over 6-48 hours.[34] Shen et al. showed that by engineering the interface of bilayer COFs, that they could increase the salt rejection. The first layer was made by an in-situ process over a period of 72 hours. The second layer a used counter diffusion method over 72 hours.[28] Xiao et al. showed that secondary growth of ACOF 1 reduced the effective pore size of the membrane at the interface via offset stacking. The membranes were synthesized over a period of 6-48 hours. [38] Wang et al. created a COF membrane at the interface of two aqueous solutions with a disparate difference in surface tension. This engineered liquid-liquid interface aligned the COF sheets as they were growing, creating very tight membranes. The membranes were synthesized over a period 1-7 days and then transferred onto PAN substrates. The resultant membrane showed over 93% NaCl rejection. [32] Wu et al. demonstrated that acetonitrile volume addition to the aqueous phase for COF membrane synthesis over 36 hours improved the crystallinity of TpPa1 and increased salt rejection.[37]

Crystallinity in COF Membranes

The theory of offset stacking of COF layers to reduce effective pore size is always illustrated using two ideal, or perfectly crystalline, COF planes. It is obvious that the membranes made using room temperature interfacial polymerization are not single crystals or an ideal flat surface. In fact, interfacial polymerization techniques are not designed for the fabrication of a 2D atom thick selective layer membrane. There is a question of whether there are unresolvable crystalline regions, the distribution and degree of crystallinity across those regions, and whether the material is completely amorphous and could still result in some significant degree of local offset stacking. That being said, the difference in length scale of two different COF materials with rigid linkers suggest that reduction in pore size distribution via stacking is still possible. An example of ideal stacking modes is shown in Figure 12.

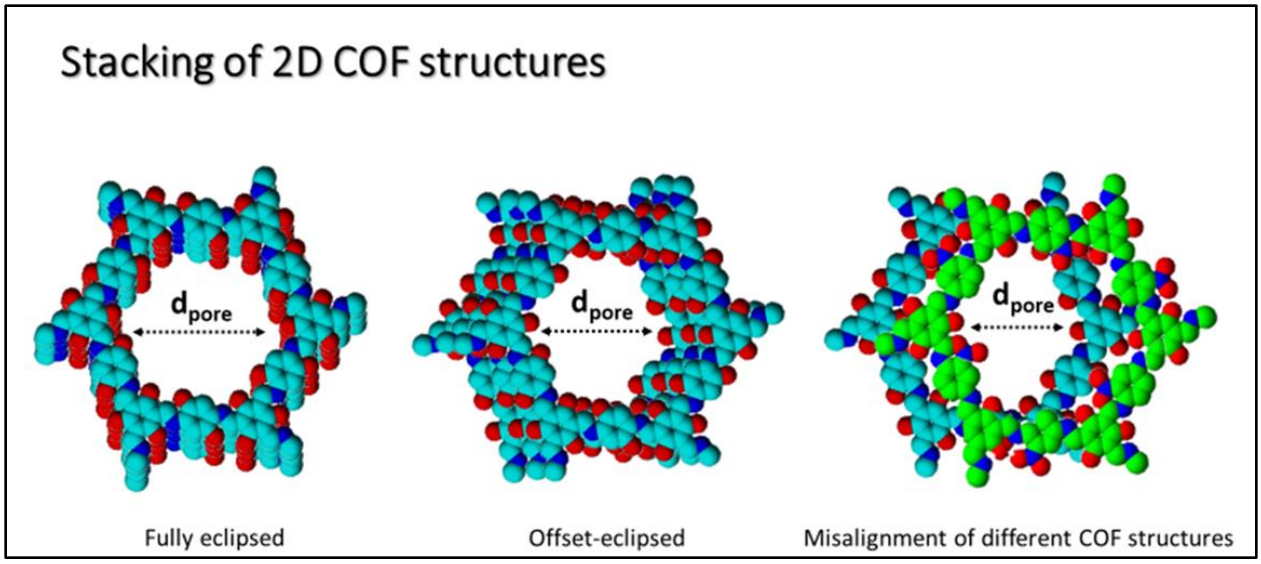

Figure 12: The figure illustrates the stacking of two layers of a covalent organic framework in an offset manner, resulting in a reduction in the effective pore size. By stacking the layers in an offset manner, the pores become misaligned, reducing the effective pore size. This can be useful in applications such as separation.

All of these advancements are great steps towards the theoretical performance of COF membranes. One reason that they all involve long reaction times is that the separation performance is affected by the crystallinity of the COFs. Room temperature COF materials exhibit lower crystallinity than simulated and solvothermally synthesized counterparts. Crystalline COF membranes are formed through an error

correction process, whereby kinetic products are reverted back into monomers, and then those monomers react again. As long as the conditions are right, this will happen repeatedly until the thermodynamically favored crystalline product is formed. Synthesis of COFs at room temperature makes the reaction less reversible than the reactions at high temperatures in solvothermal synthesis. So, in order to improve the crystal quality in room temperature synthesis, low monomer concentrations and long reaction times are used. If the reaction is stopped early, it was thought that the resultant membrane would be completely amorphous and would have to undergo some post-synthesis process to recrystallize. Feriante et al. demonstrated new insights to the crystallization mechanism of imine COF materials synthesized via the solvothermal method. They showed that within the first 60 seconds of the reaction, there were actually disordered crystalline COF sheets in solution, not amorphous COFs as previously thought. [9,13,21,39] While these studies were not operated at room temperature as COF membranes are, it begs the question that if at extreme low and long monomer concentrations and reaction times room temperature synthesis of COF membranes show some crystallinity, that at high concentrations and low reaction times, that the nucleation of COF material would have short range order in individual 2D sheets.

Scope of Work

In contrast to the previous work that has been done on COF membranes for desalination, which typically involve time-consuming processes, the current study utilizes a rapid synthesis method that has not been explored for COFs made for desalination. This significantly reduces the time required to prepare a membrane. Whereas previous methods took a minimum of 12 hours to create a membrane, the method used in this study can be completed in just seconds to minutes, depending on the COF material used. This study demonstrated reducing effective pore size by exploiting interfaces between two rapidly synthesized COF materials. This study also demonstrates the potential to further develop these materials to obtain high performing desalination membranes. The hypothesis was that the

presence of a second layer would shift the pore size distribution to increase rejection. The membrane samples were tested for their ability to remove salts from water. The characterization of the samples was done to determine the pore size distribution. The results showed that the pore size distribution and the hypothesis was supported, and salt rejection performance increased between single and dual layer membranes.

Chapter 2: Materials & Methods

Overview

Various materials were used for the synthesis of COFs and testing their performance as water filtration membranes. These materials include monomers such as p-phenylene diamine, 2,5-dimethyl-1,4-phenylenediamine, 2-nitro-1,4-phenylenediamine, 2,5-diaminohydroquinone dihydrochloride, and hydrazine hydrate, as well as tricarbaldehyde monomer 2,4,6-trihydroxybenzene-1,3,5-tricarbaldehdye and the catalyst acetic acid. Solvents deionized water and n-hexane were also used. In addition, various neutral polyethylene glycol molecules were used to determine molecular weight cut off and pore size distribution. For testing salt rejection, sodium chloride, magnesium sulfate, and sodium sulfate were used. The support membranes for the COFs were made of polyether sulfone and arrived saturated in glycerin. The COFs were synthesized using a process called interfacial polymerization, in which monomers are polymerized at the interface between two immiscible liquids. The resulting COF membranes were tested for their water flux and salt rejection properties.

Materials Used

Reagents used for COF synthesis included monomers, solvents, and catalysts. The diamine monomers include *p*-phenylene diamine <=100% (Pa-1) from Sigma Aldrich, 2,5-dimethyl-1,4-phenylenediamine >98.0% (Pa-2) from TCI, 2-nitro-1,4-phenylenediamine >98.0% (Pa-NO_2) from Sigma Aldrich, 2,5-diaminohydroquinone dihydrochloride <=100% (Pa-$(OH)_2$) from Sigma Aldrich, hydrazine

hydrate <= 90% (Hz) from Sigma Aldrich. Tricarbaldehyde monomer 2,4,6-trihydroxybenzene-1,3,5-tricarbaldehdye (Tp) from Ambeed. Catalyst, acetic acid <=100% from Sigma Aldrich. Solvents, deionized water and n-hexane >99.0% from Sigma Aldrich. The salts used for the salt rejection testing included: sodium chloride (NaCl), magnesium sulfate, and sodium sulfate. The neutral PEG molecules used in the determination of molecular weight cut off and pore size distribution included: polyethylene glycol 200 (Alfa Aesar), 300 (TCI), 600 (Alfa Aesar), 1000 (Alfa Aesar), 2000 (TCI), 4000 (TCI), 6000 (TCI), 8000 (Alfa Aesar), 10000 (Alfa Aesar), and 35000 (Sigma).

Support Membranes

The permeance of a sample is influenced by the support membranes that it is made with. Therefore, to ensure the results of these experiments are comparable, a commercially sourced UF membrane made of polyether sulfone (PES) was used for all of the support membranes. PES membranes are a beneficial material for the production of more effective membranes for water filtration and desalination. Possessing exceptional robustness and durability, PES membranes are often utilized as the substrate material when creating composite membranes, combining the advantages of PES along with supplementary materials to enhance performance. Furthermore, PES membranes can be tailored to particular needs and specifications through techniques such as surface modification or coating, enabling them to be more efficient at eliminating certain particles. Considering the great adaptability and adaptability of PES membranes, they are an ideal material for the fabrication of advanced water filtration and desalination membranes. A variety of factors can be leveraged to further modify membrane supporting membrane structure affecting properties of the COF layer. Literature also shows that the supporting membrane will have a significant impact on the formation of a selective layer synthesized via interfacial polymerization.

The support membranes arrive saturated in glycerin. Membranes are often shipped with

glycerin to protect them during transportation and storage. Glycerin is a colorless, odorless, viscous liquid that is often used as a humectant, meaning that it helps to keep materials moist. Additionally, glycerin can help to prevent the formation of cracks or other defects in the membrane, which can affect its performance. By shipping membranes with glycerin, manufacturers can help to ensure that the membranes arrive at their destination in good condition and are ready for use. Therefore, before the membranes can be used, the preservatives must be washed out. So, support membrane coupons were placed in a large water bath for at least 12 hours before they were used to make COF membranes. The support membranes were comprehensively tested to create a baseline to compare changes in performance. Moreover, NaCl, $MgSO_4$, and Na_2SO_4 solutions were used to gauge the impact of the support material on salt rejection.

Interfacial Polymerization Process

Interfacial polymerization is a process that uses two or more monomers to create thin, porous membranes at the interface between two immiscible liquids. This process is commonly used in membrane manufacture to create membranes that can effectively filter and purify water. Interfacial polymerization is also important for roll-to-roll manufacturing, which is a continuous, cost-effective method for producing materials on a moving substrate. By using this technique, it is possible to create new membrane materials that can be widely adopted for water filtration and other applications.

The COF materials that are used to make the membranes in this study are also able to take advantage of interfacial polymerization. The simple process is shown in Figure 12. The quality of the support materials and the precursor chemicals, as well as the solvent system, solubility/miscibility of reagents and catalysts, load-ability onto the substrate and temperature stability, in addition to other factors, have a significant impact on the formation of high-quality membranes made from COF. Thus, extensive experimentation aimed at optimizing such levels of these variables was undertaken in an attempt to produce membranes of an appropriate standard. The two solvents most commonly

employed in the experiment, hexane, and water, were picked for their relative commercial availability.

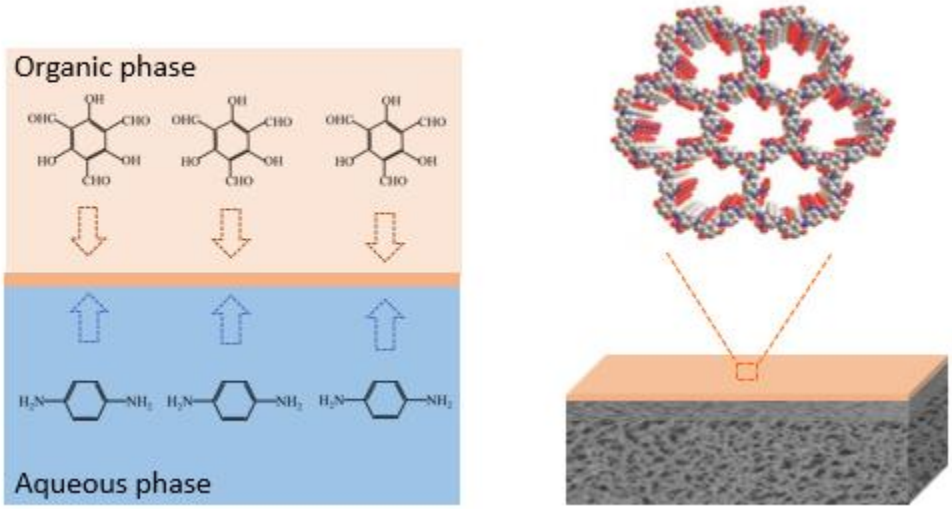

Figure 13: This figure shows the process of synthesizing a covalent organic framework using interfacial polymerization, in which monomers and a catalyst are polymerized at the interface between two immiscible liquids.

Membrane Synthesis

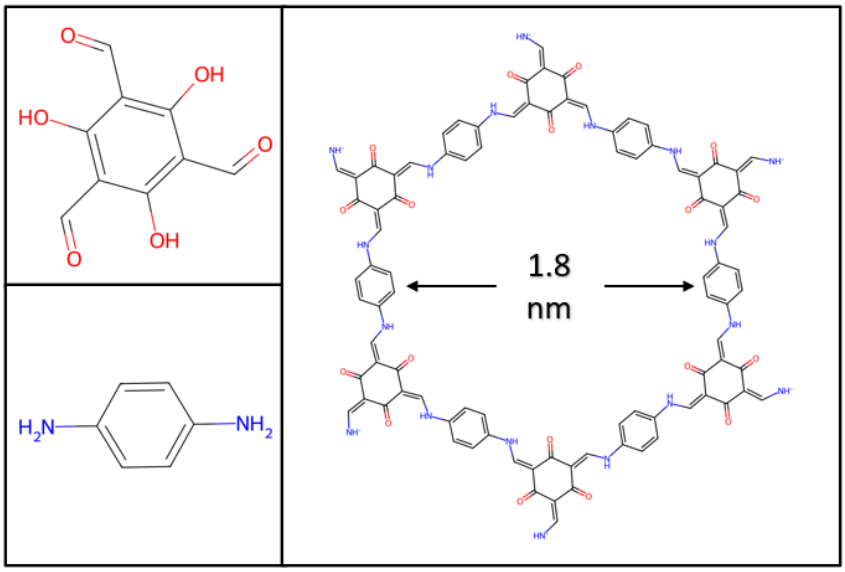

Figure 14: The figure depicts the structures of Tp and Pa, two monomers that can be used to synthesize a covalent organic framework material called TpPa1. It also shows the dimension of the pore size of TpPa1.

The synthesis of COF TFC membranes was carried out using an interfacial polymerization

method. An interface is formed between an aqueous solution, which wet the surface pores of the support membrane, and an organic solution. Figure 14 and Figures A1-A5 show the structure of these reactants. In the preparation of these solutions, first, a solution of Tp dissolved in hexane solvent was prepared by mixing the monomer and solvent at a concentration of 0.8 mmol/L. This solution was then vortexed for 30 seconds. This solution was then sonicated for 10 minutes to allow for the Tp to completely dissolve. Once this solution finished mixing, it was allowed to cool in a large room temperature water bath for 30 minutes. Next a solution of Pa-1 dissolved in water was prepared by first creating an acid solution (1.5M) by mixing glacial acetic acid to water. To this solution, Pa-1 monomer was added to achieve a concentration of 200mmol/L. This solution was then vortexed for 30 seconds. This solution was then sonicated for 10 minutes. Similar preparation methods were used to create the aqueous solutions of diamines, Pa2, Pa-NO_2, and Hz.

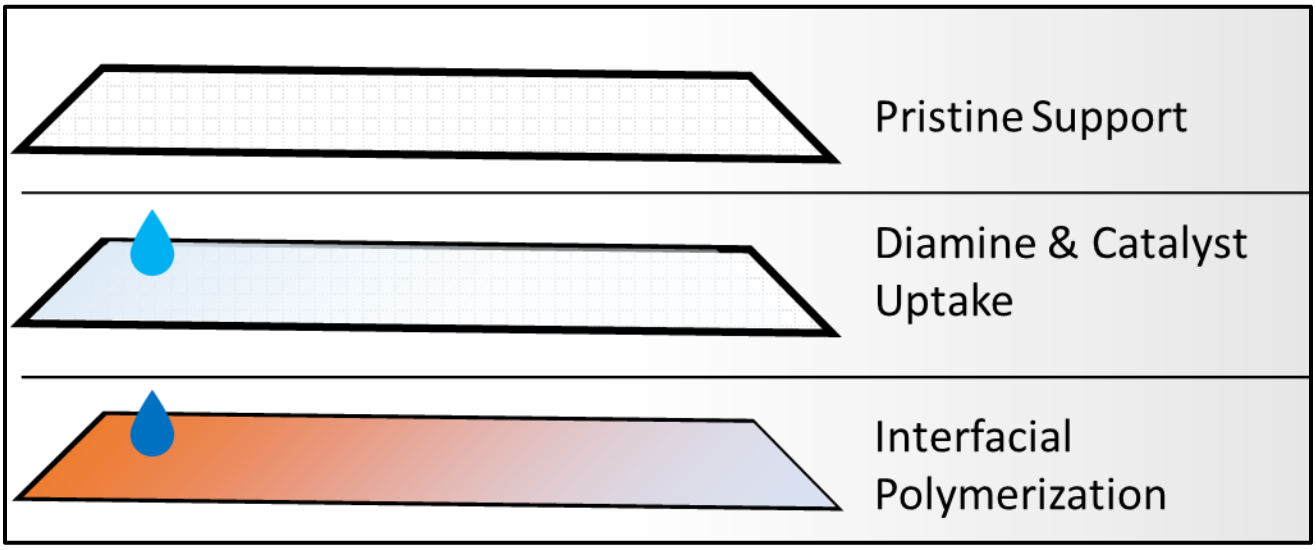

Figure 15: This figure depicts the steps involved in the interfacial polymerization synthesis of COF membranes. From top to bottom, the figure shows a pristine support membrane, the uptake of a diamine monomer and catalyst onto the support membrane, and the subsequent interfacial polymerization reaction.

Membrane Synthesis Apparatus

The membrane synthesis apparatus consists of a PTFE (polytetrafluoroethylene) tube section that seals a support membrane against a glass plate. The PTFE tube has an inner diameter of 50 millimeters and is secured to the glass slide using a clamping mechanism. When the support membrane is wetted with the aqueous reactant solution, the PFTE tube holds the organic reactant solution containing the IP reaction. The PTFE tube acts as a seal to prevent the solution from leaking and also helps to evenly distribute the solution over the support membrane. The resulting membrane is then removed from the apparatus and can be used for various applications.

Chapter 3: Experiments & Characterization

Overview

This section describes the methods used to test the performance of flat sheet membranes as water filtration systems. The testing was conducted in a crossflow configuration, in which the feed solution flows parallel to the surface of the membrane and the permeate is collected on the other side. The feed solution was pressurized by a pump and the concentration polarization was managed by controlling the ratio of permeate to concentrate flow. The membranes were tested with sodium chloride, magnesium sulfate, and sodium sulfate at 2000 mg/L at 25°C, using a crossflow velocity of 0.3 ms^{-1} and a testing pressure of 60 PSIg. The pure water permeance and solute flux of the membranes were calculated using equations based on the volume and area of the membrane, the duration of the test, and the pressure difference across the membrane. The rejection of the solutes was also calculated. Neutral solute tests were also conducted to determine the pore size distribution of the membranes. The results of these tests were used to evaluate the performance of the membranes in terms of water flux and salt rejection in the next chapter.

Cross Flow Testing Apparatus

There are two main modes of membrane testing for flat sheet membranes. One mode is the dead-end configuration in the form of a stirred cell. The membrane module for dead-end testing is constructed so that the membrane is secured in the module, and physically divides two volumes. The volume facing the surface of the membrane is the challenge solution. This solution is usually pressurized using pressurized nitrogen gas. On the other side of the membrane, is where the permeate is collected. The permeate is the solution that makes it to the other side of the membrane from the challenge solution. The challenge solution is also called the feed solution and is stirred using a stir bar and magnetic stir plate to add turbulence on the feed side of the membrane.

Concentration polarization will hamper the performance of the membrane. The membrane is designed to reject solutes. When a membrane does this, a buildup of solutes forms over the surface of the membrane. This increases the osmotic pressure that is experienced by the membrane. This decreases the transmembrane pressure experienced by the membrane, consequently reducing water flux, and reducing rejection rates. With dead-end cells, this problem is addressed by stirring the feed solution, introducing turbulence that reduce the concentration of solutes at the surface of the membrane.

In the crossflow configuration, it is easier to manage concentration polarization by changing the dimension of the feed channel or by increasing the crossflow velocity with an increase in flow rate. The feed solution is pressurized by a pump which is drawing the feed from a reservoir. The feed solution runs parallel to the surface of the membrane, and the feed solution that has been concentrated by the membrane flows back to the reservoir. The concentration polarization is further mitigated by controlling the ratio of permeate to the ratio of concentrate flow to maintain low water recovery.

The crossflow configuration was chosen for the experiments. The pumps are diaphragm pumps

from Aquatec that are rated for continuous flow. The crossflow cell was designed in house and manufactured by Xometry. The flow channel was designed to test membranes that are 2.5 by 2.5 cm. The channel height of the feed flow is 2 mm. Polypropylene tubing and push to connect fittings were used to connect all components of the apparatus. Pressure was monitored using a two pressure gauges.

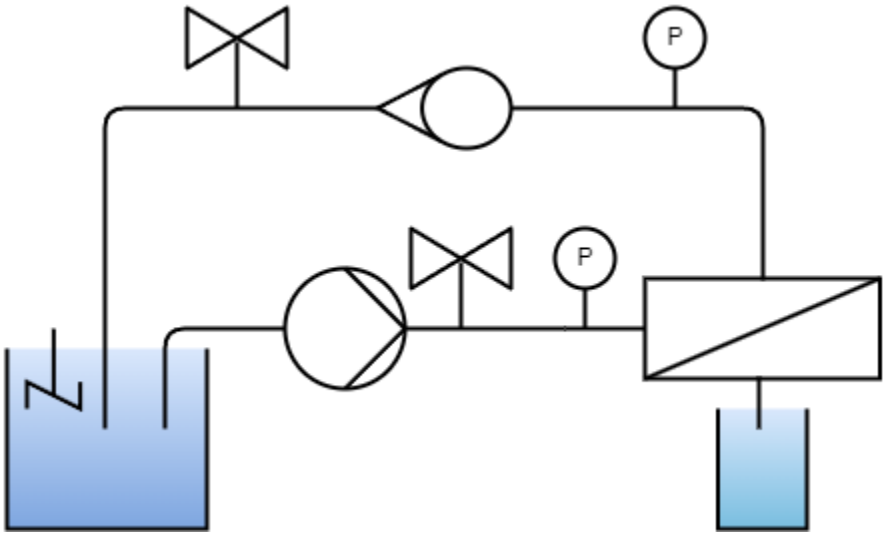

Figure 16: Piping and instrumentation for the crossflow membrane testing apparatus. The diagram illustrates the various components of the apparatus, including the reservoir, pump, pipes, and pressure gauges, membrane, and rotameter, and how they are connected to form the complete system

Salt Testing Parameters

The salt rejection testing was conducted using the crossflow mode. The membranes were challenged with NaCl, $MgSO_4$, and Na_2SO_4 at 2000 mg/L at 25°C. The membranes samples were tested using 2 replicates using a cross flow velocity of 0.3 ms^{-1}. The water recovery of the membranes was kept low to keep the concentration as close to the starting value as possible. Conductivity measurements of the feed at the start of the test, of the feed at the end of the test, and three samples of permeate from the feed were used to determine the membrane performance. Before salt testing the membranes, they were subjected to compaction with pure water at 100 PSIg for 30 minutes to stabilize the membrane. The applied testing pressure for the membranes was set to 60 PSIg. Conductivity was measured using a

conductivity meter, and flux was measured gravimetrically using a scale. Measured values were used to calculate rejection and pure water permeance. Were J_w is water flux in $Lh^{-1}m^{-2}$. A_m is the area of the membrane, t is time, and V is volume of the permeate. A is pure water permeance, and ΔP is the transmembrane pressure in bar. R is the rejection in percent. C_p is the concentration of the permeate and C_f is the concentration in the feed solution.

$$J_w = \frac{V}{A_m \times t} \tag{1}$$

$$A = \frac{V}{A_m \times t \times \Delta P} \tag{2}$$

$$R(\%) = \left(1 - \frac{C_P}{C_f}\right) \times 100 \tag{3}$$

Neutral Solute Tests

Neutral solute testing will give better understanding of the pore size distribution. Since the molecules are not charged, the contribution of electrostatic mechanisms of rejection are not prominent. Low (25mg/L) concentration solutions of PEGs of 9 different molecular weights were prepared. Then the membranes were challenged with said solutions. Just like in the salt experiments, all relevant samples were collected in order to calculate rejection. All samples were analyzed for total organic carbon. Since the TOC-L detects measures of carbon, the calculation for rejection can be made directly. A lognormal probability density model for pore size distribution with a pore size correction factor of 0.416 was used to relate the rejection of these solutes to a pore size distribution. Prior to the development of pore size distribution functions, there were several methods that were commonly used to estimate the average pore size of a material by using data from rejection of neutral solutes. These methods only were able to estimate an average pore size, which is not enough data to describe pore size well.

The Einstein-Stokes radius is a value that is calculated using the Einstein-Stokes equation, which is a mathematical relationship that describes the motion of a small particle suspended in a fluid. This equation can be used to determine the size of a particle. For PEGs the Stokes radius is described by equation 4. Where D_s is the stokes diameter, M is the molecular weight of the neutral solute. μ_p is the mean pore size determined at 50% rejection. σ_p Is the ratio between the mean pore size and pore size at the rejection of 84.13%.

$$D_s = 33.46 \times 10^{-3} \times M^{0.557} \tag{4}$$

$$\frac{dR(d_p)}{d\,d_p} = \frac{1}{d_p\, ln\, \sigma\sqrt{2\pi}} exp\left[-\frac{\left(ln\, d_p - ln\, \mu_p\right)^2}{2\left(ln\, \sigma_p\right)^2}\right] \tag{5}$$

For the neutral solute rejection testing of the membranes, the membranes are first compacted at 100 PSIg for 30 minutes before the testing begins. The membrane is then subjected to a range of polyethylene glycol (PEG) solutions with diverse molecular weights. For each PEG solution, the membrane's rejection is measured by from 3 samples of permeate and recording the results. The collected data is used to generate a molecular weight cut-off (MWCO) curve, which plots the molecular weight of the PEG solutions on the x-axis and the rejection of the membrane on the y-axis. This curve illustrates the relationship between the molecular weight of the PEG probes and their ability to permeate the membrane. A log normally distributed probability density function (PDF) can be created from the MWCO curve data, which depicts the relative probability of various pore diameters within the membrane. Higher probability density indicates that those pore diameters are more likely to exist in the membrane. MWCO data plotted as rejection vs solute size can be used to represent pore size distribution using a log-normal distribution. This was also verified for other porous membranes, and it is

used for characterizing NF membranes as well. Pore size distribution methods plot MWCO using stokes radii rather than molecular weight. The data follows a linear relationship when the Log values are plotted. The median rejection and geometric standard deviation rejection from the fitted data are then input into a function to produce a log normal distributed probability density function.

Chemical Characterization

FTIR, or Fourier Transform Infrared spectroscopy, is a technique used to analyze the vibrational, rotational, and other low-frequency modes in a material. It is often used to identify the functional groups present in a material, as well as to determine its chemical composition and purity.

Structural Characterization

SEM was used on all the samples to obtain high resolution images of the surface of the membranes. The membranes that were made were unable to be sectioned via conventional freeze fracture, or cryo-snap methods. Thus, only surface images of all membranes were obtained for membranes.

Chapter 4: Results & Discussion

Properties of Membranes

Photos

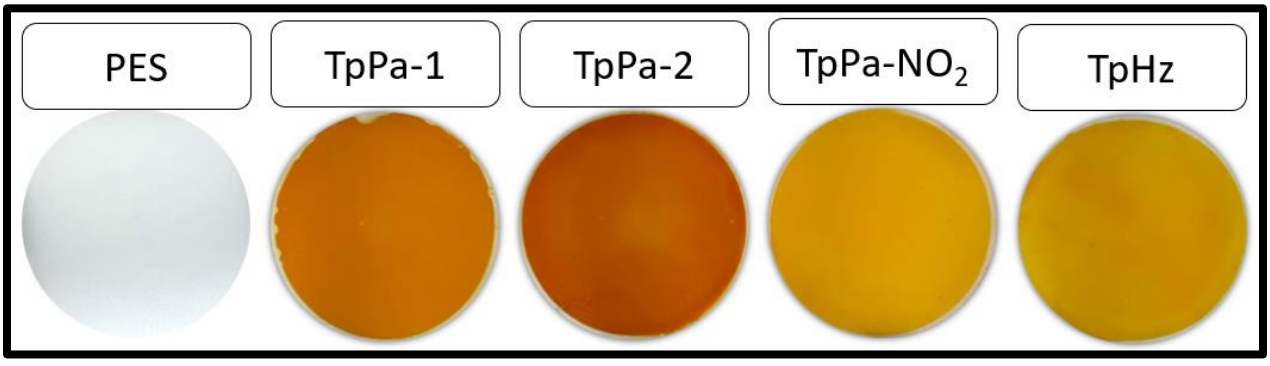

Figure 17: Cropped photos of PES substrate and single layer covalent organic framework membranes, labeled TpPa1, TpPa2, $TpPaNO_2$, and TpHz

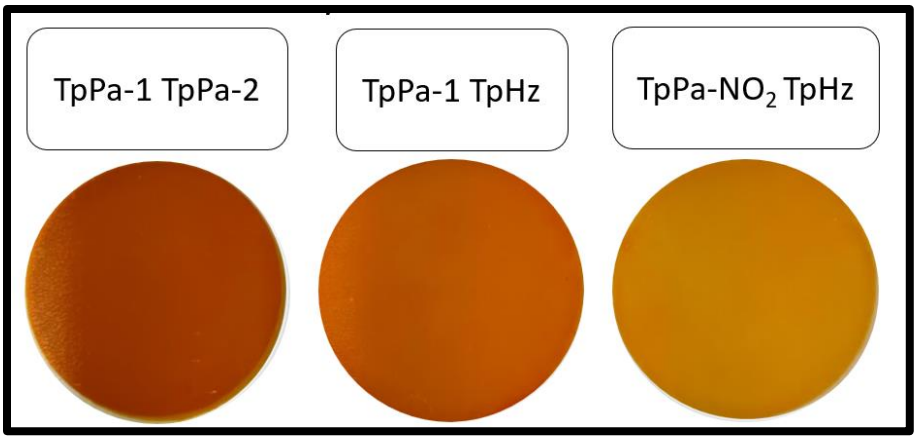

Figure 18: Cropped photos of three dual layer COF membranes, labeled $TpPaNO_2$-TpHz, TpPa1-TpHz, and TpPa1-TpPa2

Figures 17 and 18 provided visual representations of the membranes. Figure 17 displays a photo of the pristine polyether sulfone substrate that was used to make the COF membranes, as well as the single layer membranes TpPa-1, TpPa-2, TpPa-NO_2, and TpHz These single layer membranes all appear to take on some shade of yellow or orange. In Figure 18, the dual layer membranes made from the single layer membranes, TpPa-1 + TpPa-2, TpPa-1 + TpHz, TpPa-NO_2 + TpHz, are all much darker than their single layer counterparts, with deep orange colors. This change in color is a good indicator of successful membrane formation.

FTIR

In the FTIR experiments, identification of 4 COF materials was targeted: TpPa-1, TpPa-2, TpPa-NO_2, and TpHz. We focused on identifying the C-N, C=C, and C=O vibrations, as well as the NO_2 vibration in $TpPaNO_2$. The C-N vibration was found at approximately 1250 cm^{-1}, the C=C vibration at around 1560 cm^{-1}, and the C=O vibration at around 1600 cm^{-1} for all COF materials. Additionally, the NO_2 functional group, which is composed of a nitrogen atom double-bonded to an oxygen atom and a single bond to another oxygen atom, was found in $TpPaNO_2$ at 1506 cm^{-1}, confirming the presence of $TpPaNO_2$.

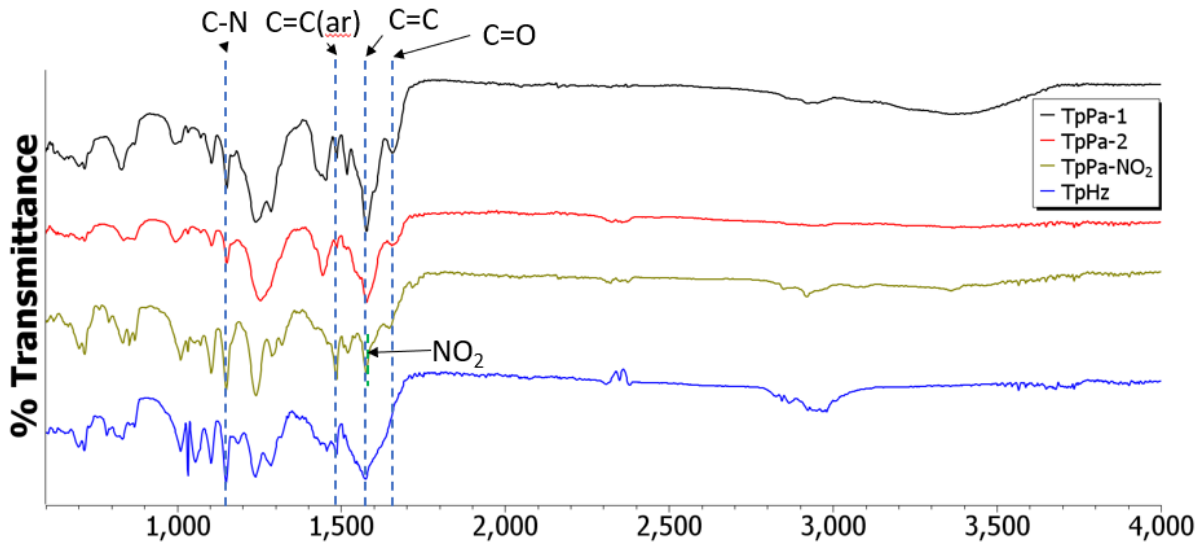

Figure 19: This figure presents the Fourier transform infrared (FTIR) spectra of four single layer covalent organic framework membranes, labeled TpPa1, TpPa2, TpPaNO_2, and TpHz

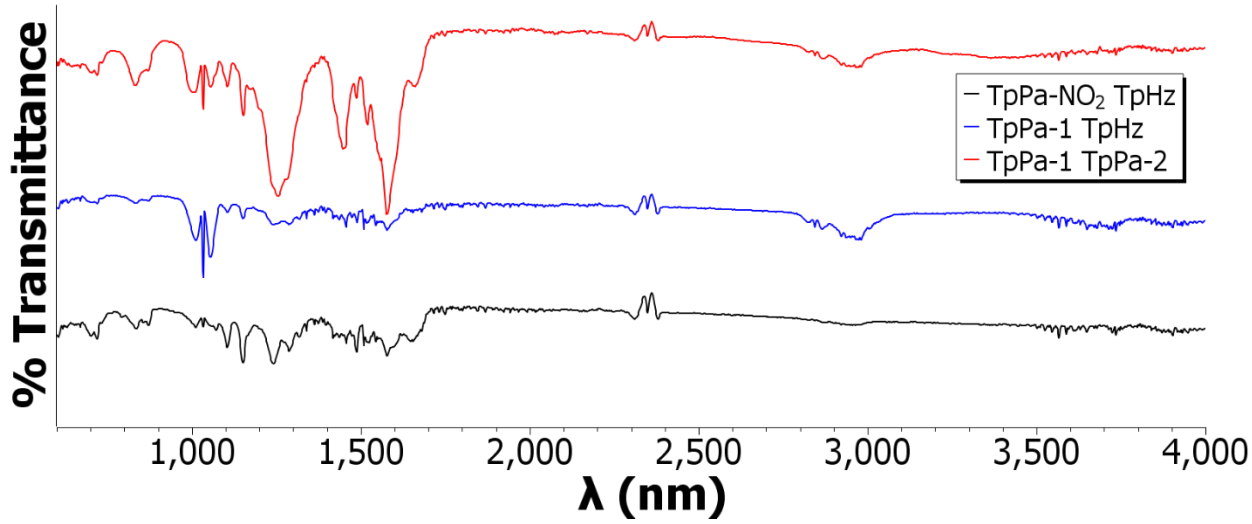

Figure 20: This figure displays the FTIR spectra of three dual layer COF membranes, labeled TpPaNO_2-TpHz, TpPa1-TpHz, and TpPa1-TpPa2

When the two materials were scanned at the same time in the dual-layer membrane, signatures from both materials appeared in the spectra, confirming the presence of both materials in the double layer material. These results confirm the presence of the expected bonds in the sample and provide evidence that the targeted COF materials were indeed synthesized as membranes. These results are consistent with our expectations. The deep colors that formed during the synthesis of the single layer

and dual layer membranes also show that there was successful formation of COF material.

Confocal Microscopy

In this study, the thicknesses of single layer and dual layer COF membranes were characterized using confocal microscopy. The results showed that the thickness of the single layer membranes varied from 250 to 326 nm, with TpPa-1 having a thickness of 252 nm, TpPa-2 of 326 nm, TpPa-NO_2 of 250 nm, and TpHz of 330 nm.

When two single layer membranes were combined to form a dual layer membrane, the overall thickness of the resulting membrane increased. For example, the dual layer membrane TpPa-1 + TpPa-2 had a thickness of 426 nm, while the dual layer membrane TpPa-1 + TpHz had a thickness of 552 nm. The dual layer membrane TpPa-NO_2 + TpHz had a thickness of 418 nm.

The confocal microscope depth scan function was used to make these measurements. Figure 21 and 22 show images of the films prepared from the aforementioned membranes. The confocal microscope is a powerful tool for the characterization of thin film samples like these COF membranes, as it allows for non-destructive 3D imaging of the samples and provides detailed information about the thickness. The thickness of these COF membranes has important implications for their performance in desalination applications. By understanding how to control the thickness of COF membranes to create high quality thin membranes, the desalination performance of the membranes can be enhanced.

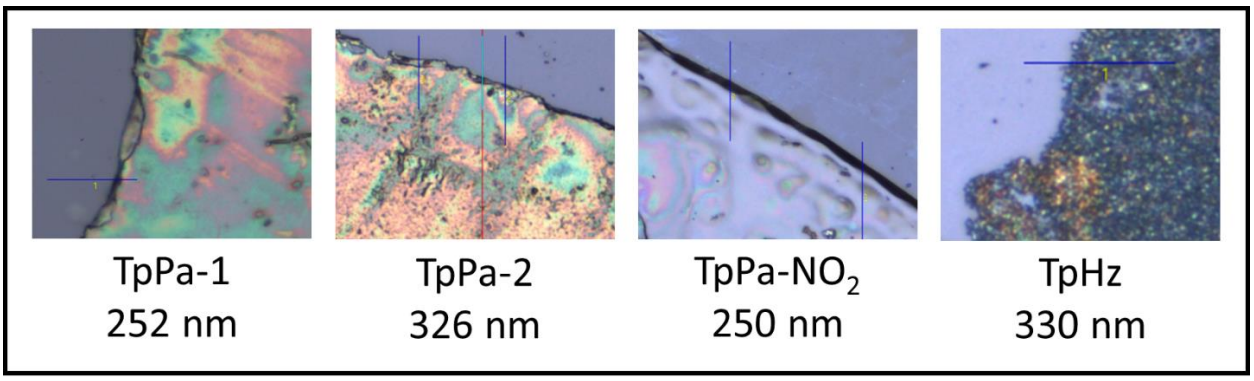

Figure 21: confocal microscope depth scans for single layer covalent organic framework membranes.

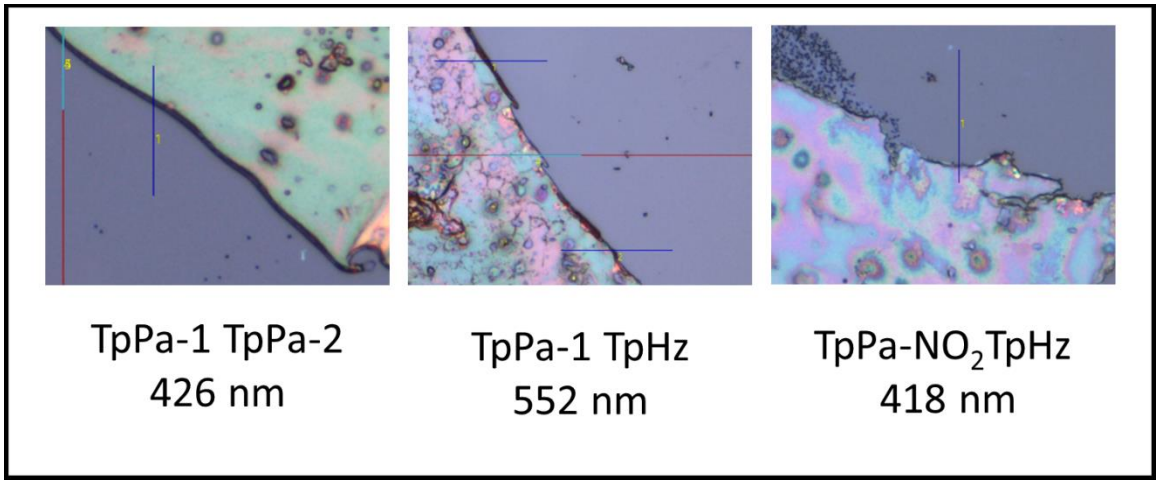

Figure 22: confocal microscope depth scans for single layer covalent organic framework membranes.

SEM

The results of the scanning electron microscope (SEM) characterization of the single layer and dual layer COF membranes are presented in figures 21-28. These figures show the surface morphology of the membranes, providing insight into their pore structure and overall film integrity. Upon examination of the SEM images, it can be observed that the surface morphology of the single layer COF membranes, TpPa-1, TpPa-2, TpPa-NO_2, and TpHz, is relatively similar. The images show a porous surface structure. The images show a continuous and smooth COF membrane on the support surface without distinctive morphological features.

When comparing the dual layer COF membranes TpPa-1 + TpPa-2, TpPa-1 + TpHz, TpPa-NO_2 + TpHz, to their single layer counterparts, a noticeable difference in the surface morphology can be observed. The dual layer membranes exhibit a denser surface structure. This can be attributed to either that the second layer, when synthesized on top of the first, has filled in some of the pores and channels, creating a more continuous film, or that the single layer COF membranes were damaged by the SEM

because the film was thinner and more susceptible to damage by the electron beam over large substrate pores.

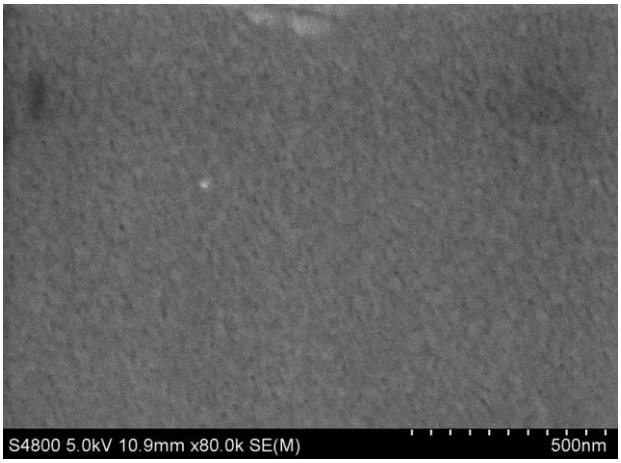

Figure 23: SEM image of the PES support membrane surface.

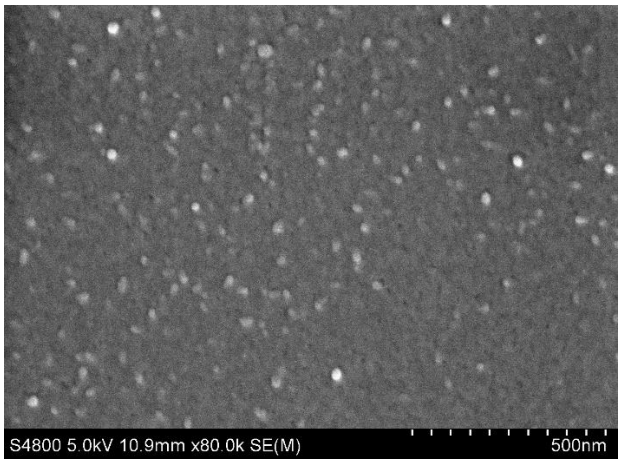

Figure 24: SEM image of the TpPa1 COF membrane surface.

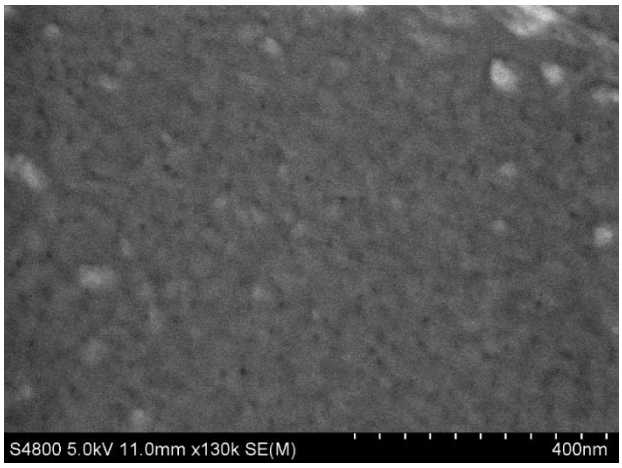

Figure 25: SEM image of the TpPa2 COF membrane surface.

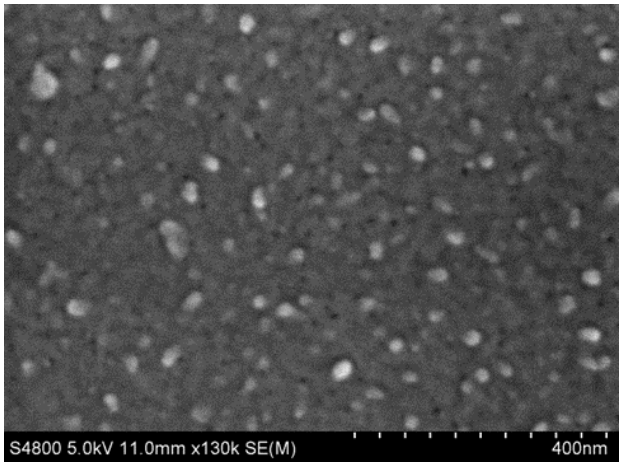

Figure 26: SEM image of the TpPa-NO_2 COF membrane surface.

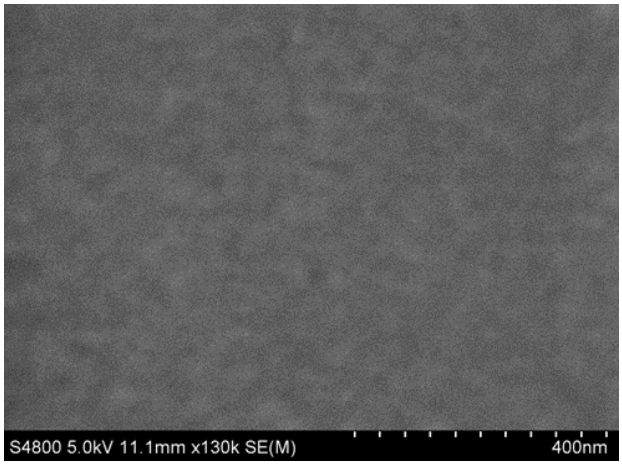

Figure 27: SEM image of the TpPa-$(OH)_2$ COF membrane surface.

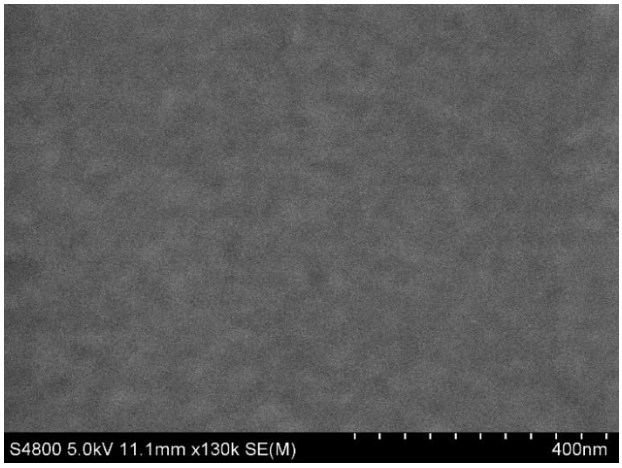

Figure 28: SEM image of the TpHz COF membrane surface.

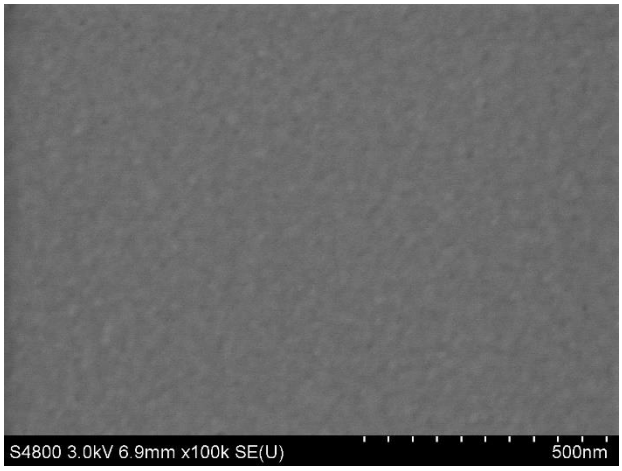

Figure 29: SEM image of the TpPa1-TpPa2 COF membrane surface.

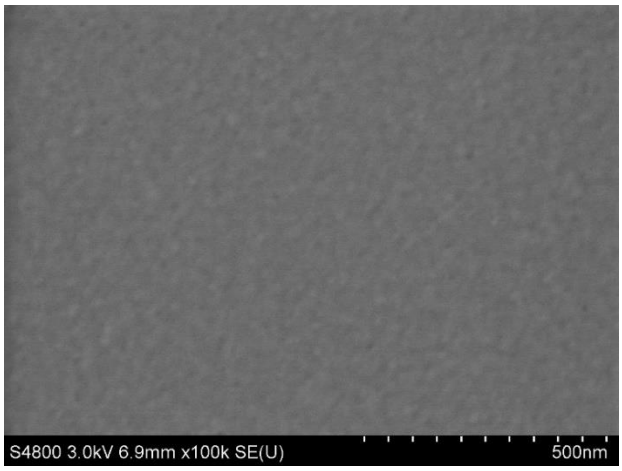

Figure 30: SEM image of the TpPa1-TpHz COF membrane surface.

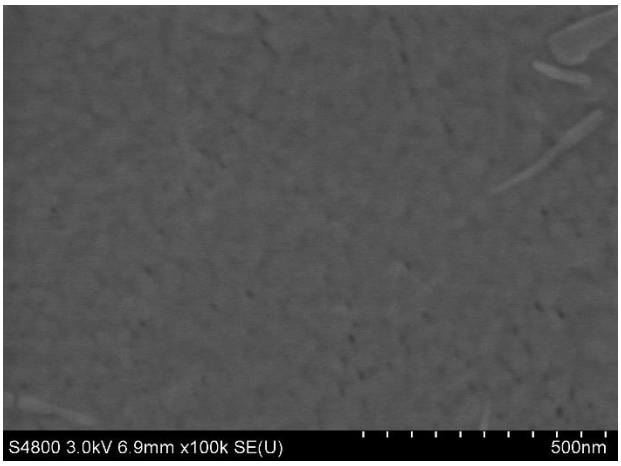

Figure 31: SEM image of the TpPa-NO_2-TpHz COF membrane surface.

Pore Size Distribution

In order to more accurately characterize the separation performance of the membranes studied in this work, neutral solute rejection was fit to create pore size distribution graphs as described in Chapter 3. These graphs provide a more detailed view of the size and distribution of the pores in the membranes, which can be used to better understand their separation behavior.

The pore size distribution graphs for the single layer membranes are shown in Figure 32-36. As can be seen in the figure, the pore size distribution for each membrane exhibits a unique range of pore sizes, and all are broad distributions with a mix of small and large pores.

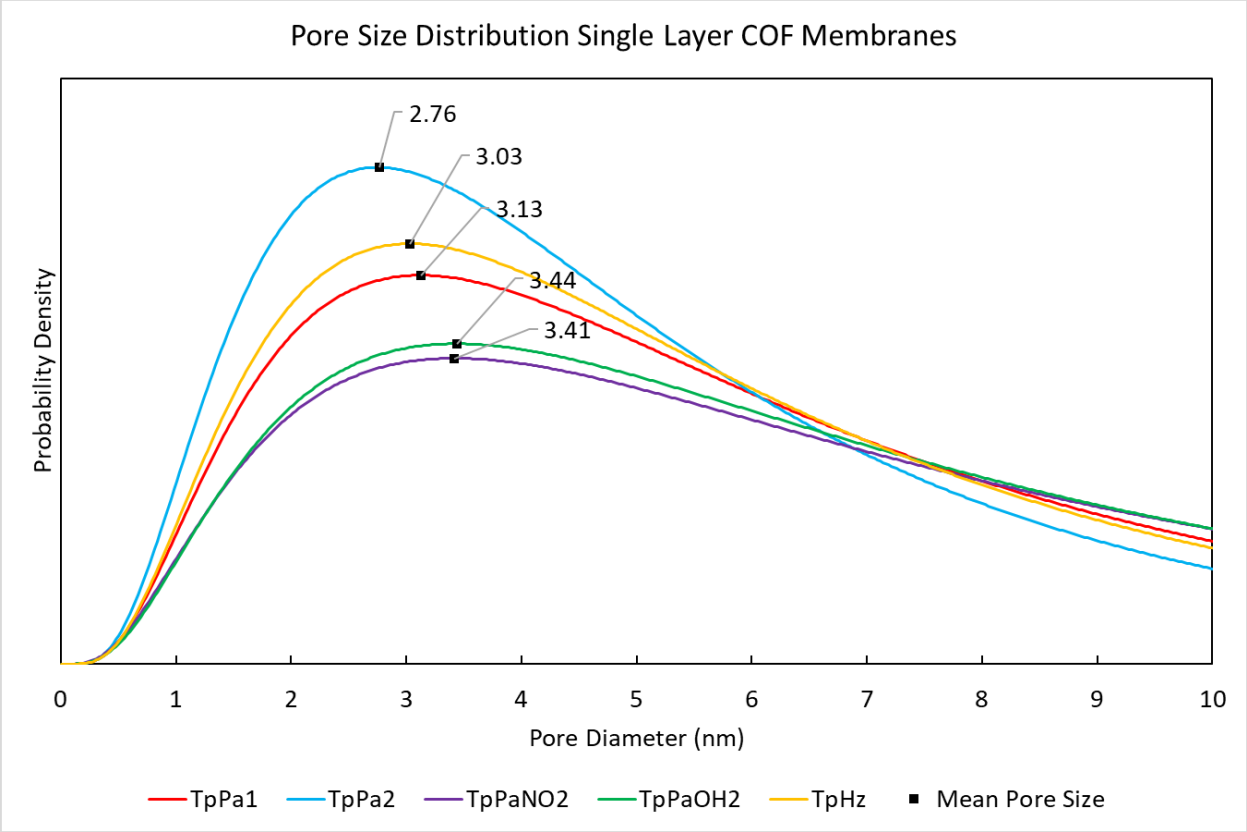

Figure 32: This figure presents the pore size distribution of five single layer COF membranes. TpPa1, TpPa2, $TpPaNO_2$, $TpPa(OH)_2$, and TpHz.

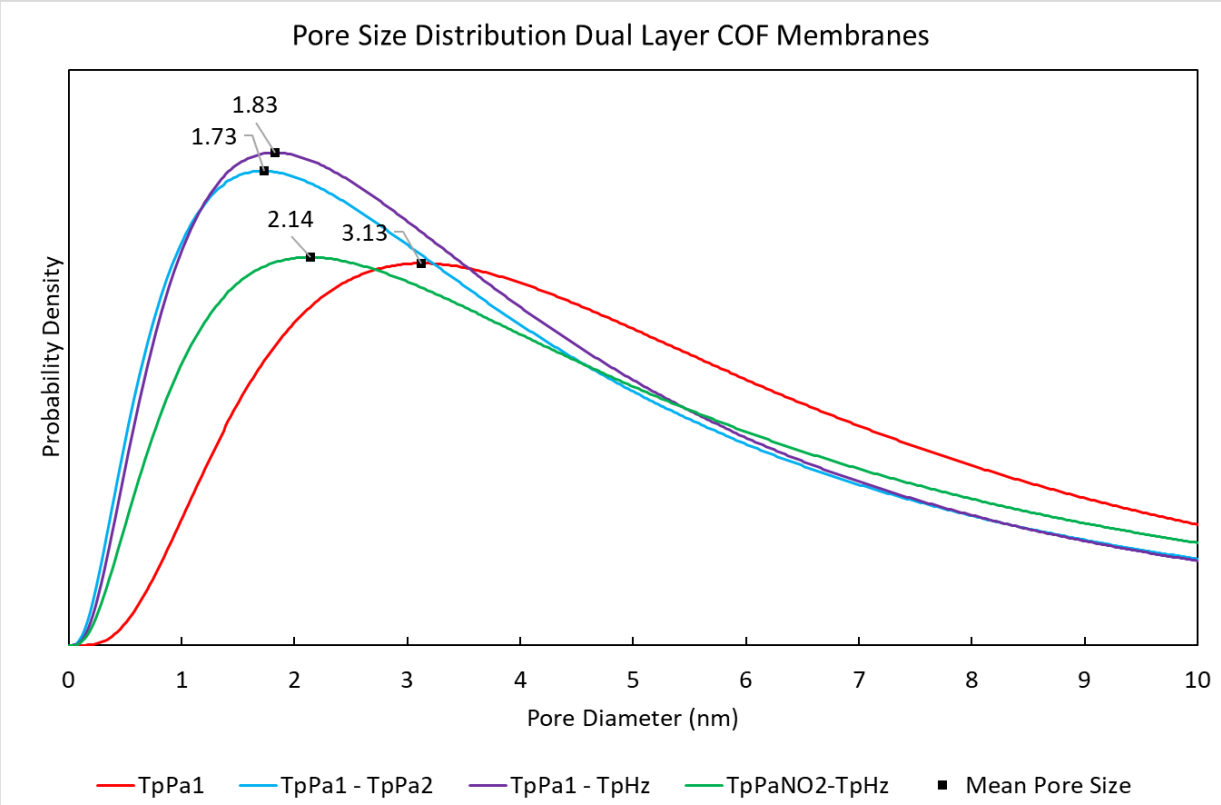

Figure 33: This figure presents the pore size distribution of dual layer COF membranes. TpPa1- TpPa2, TpPaNO_2-TpHz, TpPa1-TpHz.

Single-layer TpPa1 had a mean pore size of 3.13 nm. This value is sits around the center for the single COF layer membranes tested. A larger mean pore size suggests a membrane may exhibit higher flux but may also lead to a lower rejection of solutes. TpPa$(OH)_2$ had a mean pore size of 3.44 nm, which is the largest of all the membranes studied, followed by TpPaNO_2, 3.41 nm, TpPa1, 3.13 nm, TpHz, 3.03 nm, and TpPa2, 2.76 nm, the lowest of the single-layer membranes.

Overall, the mean pore size values of the five single layer COF membranes studied varied slightly, with a range of 3.44 nm to 2.76 nm. As opposed to a narrower distribution, the quality of the mean pore size probability density functions resembles broad distributions, which corresponds to a common membrane morphology with variable pore sizes.

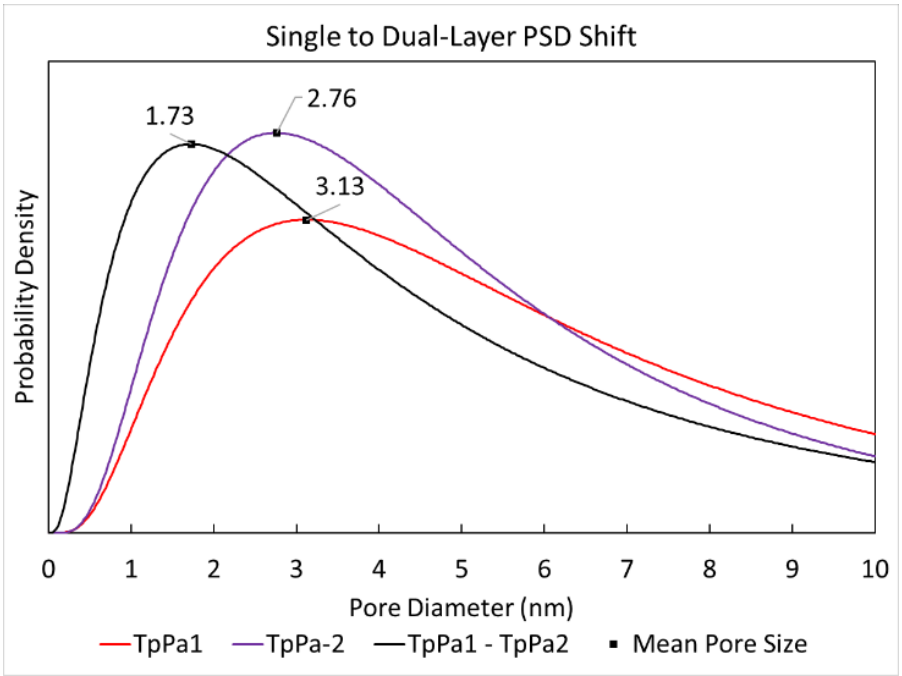

Figure 34: This figure presents the pore size distribution shift when combining TpPa1 and TpPa2

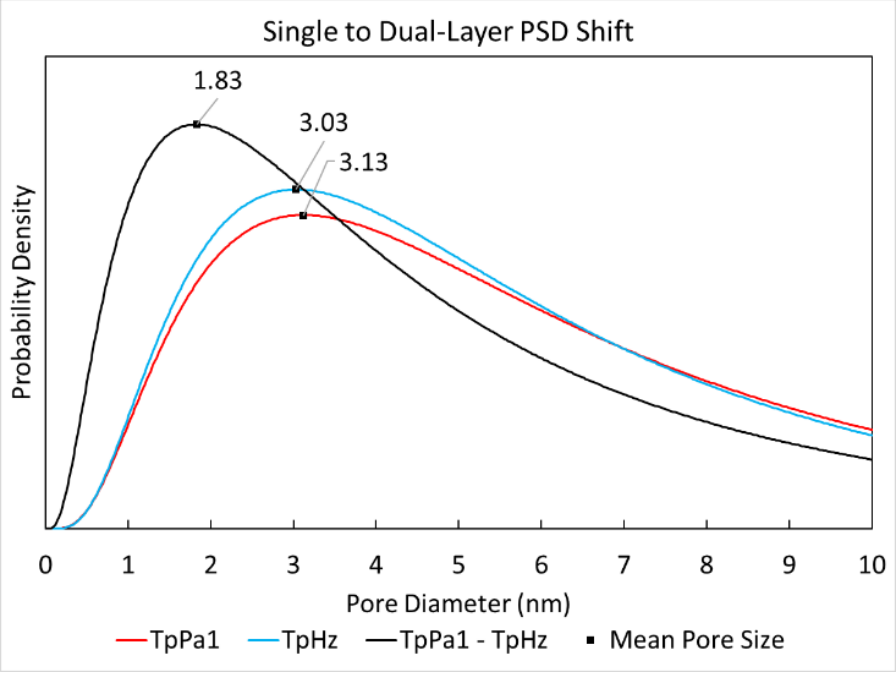

Figure 35: This figure presents the pore size distribution shift when combining TpPa1 and TpHz

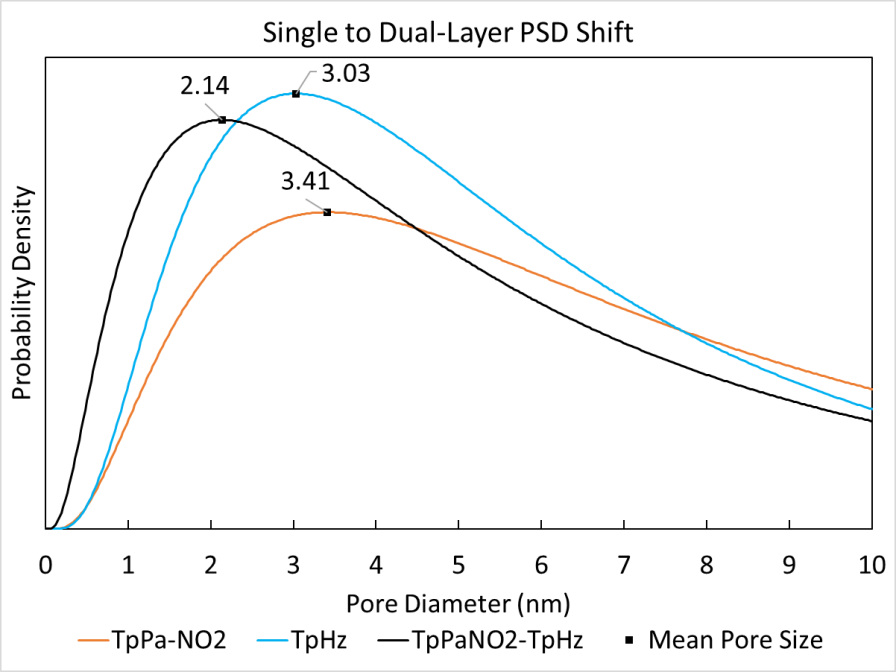

Figure 36: This figure presents the pore size distribution shift when combining $TpPaNO_2$ and TpHz

The results show that there is a shift in the pore size distribution from single layer to dual layer membranes. Specifically, the dual layer membranes exhibit a lower mean pore size than their single layer counterparts. This shift in pore size distribution is likely the main reason for the observed enhancement in salt rejection with dual layer membranes compared to single layer membranes.

In summary, the results show that the pore size distribution is a critical parameter that plays a key role in determining the performance of the COF membranes, in this case the dual layer membranes show a shift in the pore size distribution towards smaller pore size that is responsible for the enhancement in salt rejection when compared to single layer membrane, which is relevant in desalination. However, more studies are needed to understand the mechanism behind this shift and optimize the synthesis conditions to get the desired pore size distribution for specific application.

Water Contact Angle

In order to investigate the wetting behavior of the membranes studied in this work, water

contact angle measurements were performed. The water contact angle is a measure of the angle formed between the water droplet and the membrane surface and is a useful parameter for understanding the wettability and hydrophobicity/hydrophilicity of the membranes.

The water contact angle measurements for the membranes are shown in Figure 37. As can be seen in the table, the water contact angles for the membranes range from 45° for TpPaNO_2 to 71.2° for TpHz. The water contact angle is generally indicative of the hydrophobicity/hydrophilicity of the membrane, with smaller angles indicating more hydrophilic surfaces and larger angles indicating more hydrophobic surfaces.

Membrane	Water Contact Angle		
TpPa-1	58.1	+/-	1
TpPa-2	60.3	+/-	2.4
TpPa-NO2	45	+/-	2.2
TpHz	71.2	+/-	0.8
TpPa-1 + TpPa-2	61.4	+/-	5.3
TpPa-1 + TpHz	60	+/-	0.5
TpPa-NO2 + TpHz	65	+/-	2.4

Figure 37: This figure illustrates the water contact angle of four single layer membranes and two dual layer membranes. The water contact angle is a measure of the wetting behavior of a surface, with higher values indicating a more hydrophobic surface and lower values indicating a more hydrophilic surface.

Performance of Membranes

In order to evaluate the separation performance of the membranes studied in this work for salt solutions, pure water flux and salt rejection tests were performed using three different salts: NaCl, $MgSO_4$, and Na_2SO_4. The pure water flux was calculated according to equation (2), and the salt rejection was calculated as the percentage of salt ions that were retained by the membrane, equation (3).

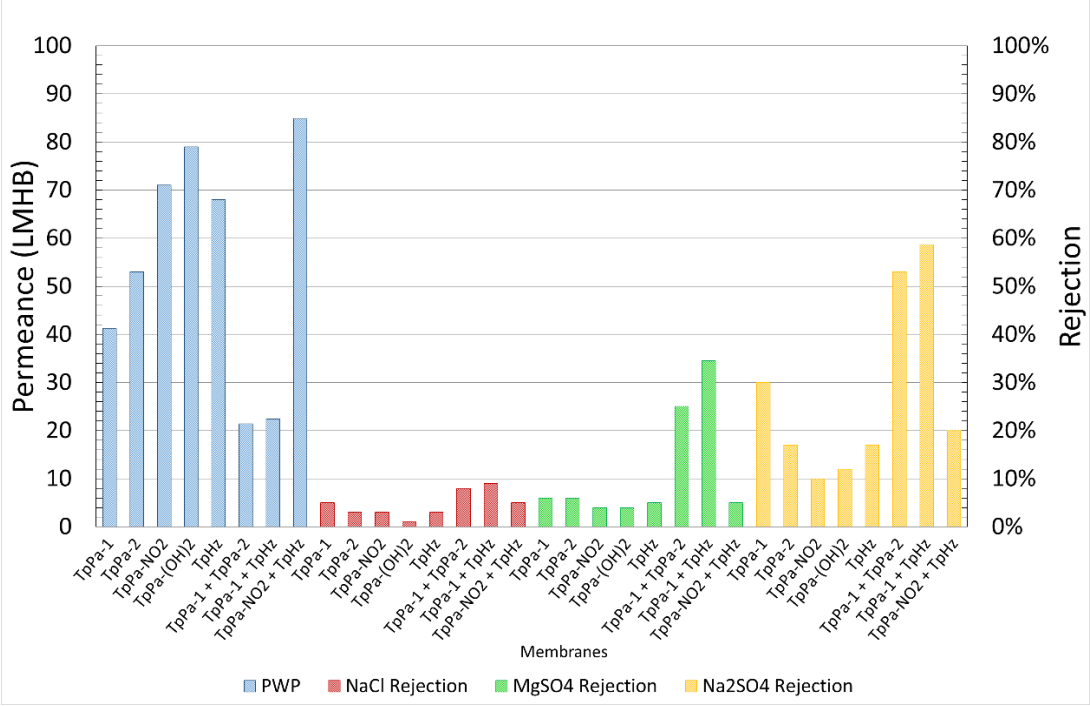

Figure 38. Salt Rejection Performance of Single and Dual Layer COF Membranes on PES

Pure water flux and salt rejection of the membranes vary depending on the COF membrane material. The single layer membranes have lower salt rejection and higher water flux, while the dual-layer membranes show lower pure water flux, but enhanced salt rejection. The dual-layer membranes displayed in figure 38 perform better than their individual layers as single layer membranes. These results suggest that the separation performance of the membranes is influenced by the combination of materials that are used to make the dual-layer membrane. In addition to this, it also shows that the dual layers have enhanced salt rejection over the single layer membranes.

Summary

The separation performance of the membranes was evaluated using neutral solute rejection experiments and analyzed using pore size distribution curves. The pore size distributions of dual-layered membranes shifted to smaller pore sizes. The wetting behavior of the membranes was characterized using water contact angle measurements. All membranes exhibited similar wetting behavior, except for TpPa-NO_2.The separation performance of the membranes for salt solutions was evaluated using pure

water flux and salt rejection tests. The dual-layer membranes exhibited higher Na_2SO_4, $MgSO_4$, and NaCl rejection than the single-layer membranes. The dual-layer membranes also exhibited decreased flux. Even with a decrease in flux, the dual-layer membrane still performed better than the single-layer membranes.

Chapter 5: Conclusions

Single layer membrane becomes darker with the synthesis of a second layer over top of the first. This change in color and the increase in membrane thickness are evidence for the formation of a new layer formed over the first layer. FTIR signatures from both COF materials are present in the spectrum, indicating the presence of two COF materials on the dual layer membranes.

Based on the findings of this study, the introduction of a second layer in COF membranes has shown to be successful in achieving an increase in performance. Analyzing both the rejection and pure water permeance, the performance of dual layer membranes has surpassed that of the single layer membranes made in this study. Furthermore, the introduction of a second layer did also significantly shift the pore size distribution. There is potential to reduce the effective pore size even further and make desalination even more efficient. From the results of this research, it can be concluded that rapidly synthesized dual-layer COF membranes enhance the desalination performance of COF membranes, and they hold potential for further improvement.

Chapter 6: Future Work

Minimizing Thickness and Narrowing Pore Size Distribution

One important area of research is the minimization of membrane thickness. As the thickness of the membrane decreases, the water permeance of the membrane will increase. Investigations on various techniques for reducing the thickness of COF membranes, such as the selection of a support membrane with high pore density or modifying the synthesis process to create thinner membranes with the addition of reactive and or nonreactive species that help modulate and increase the quality of COF

membranes. Additionally, quantification of how well one COF material interacts with another COF material to reduce effective pore size, as well as how this varies with degree of crystalline or amorphous nanostructures, and varied morphology should also be considered. This would provide deeper insight into how these factors influence the efficiency of COF membrane technology. Moreover, integrating more continuous layers of COF membranes and techniques to enhance long range order of COF membranes may further increase the efficiency of this technology.

Bibliography/Works Cited/References

1 Abbott, B. W., Bishop, K., Zarnetske, J. P., Minaudo, C., Chapin, F. S., Krause, S., Hannah, D. M., Conner, L., Ellison, D., Godsey, S. E., Plont, S., Marçais, J., Kolbe, T., Huebner, A., Frei, R. J., Hampton, T., Gu, S., Buhman, M., Sara Sayedi, S., Pinay, G. (2019). Human domination of the global water cycle absent from depictions and perceptions. Nature Geoscience, 12(7), 533–540. https://doi.org/10.1038/s41561-019-0374-y

2 Anis, S. F., Hashaikeh, R., & Hilal, N. (2019). Reverse osmosis pretreatment technologies and future trends: A comprehensive review. Desalination, 452, 159–195. https://doi.org/10.1016/j.desal.2018.11.006

3 Arqueros, C., Zamora, F., & Montoro, C. (2021). A Perspective on the Application of Covalent Organic Frameworks for Detection and Water Treatment. Nanomaterials, 11(7), 1651. https://doi.org/10.3390/nano11071651

4 Böddeker, K. W. (2008). Liquid separations with membranes: An introduction to barrier interference. Springer.

5 Castelletto, S., & Boretti, A. (n.d.). Advantages, limitations, and future suggestions in studying graphene-based desalination membranes. RSC Advances, 11(14), 7981–8002. https://doi.org/10.1039/d1ra00278c

6 Cote, A. P., Benin, A. I., Ockwig, N. W., O'Keeffe, M., Matzger, A. J., & Yaghi, O. M. (2005). Porous, Crystalline, Covalent Organic Frameworks. 310.

7 Dey, K., Pal, M., Rout, K. C., Kunjattu H, S., Das, A., Mukherjee, R., Kharul, U. K., & Banerjee, R. (2017). Selective Molecular Separation by Interfacially Crystallized Covalent Organic Framework Thin Films. Journal of the American Chemical Society, 139(37), 13083–13091. https://doi.org/10.1021/jacs.7b06640

8 Eke, J., Yusuf, A., Giwa, A., & Sodiq, A. (2020). The global status of desalination: An assessment

of current desalination technologies, plants and capacity. Desalination, 495, 114633. https://doi.org/10.1016/j.desal.2020.114633

9 Feriante, C., Evans, A. M., Jhulki, S., Castano, I., Strauss, M. J., Barlow, S., Dichtel, W. R., & Marder, S. R. (2020). New Mechanistic Insights into the Formation of Imine-Linked Two-Dimensional Covalent Organic Frameworks. Journal of the American Chemical Society, 142(43), 18637–18644. https://doi.org/10.1021/jacs.0c08390

10 GebreEgziabher, M., Jasechko, S., & Perrone, D. (2022). Widespread and increased drilling of wells into fossil aquifers in the USA. Nature Communications, 13(1), Article 1. https://doi.org/10.1038/s41467-022-29678-7

11 Ghaffour, N., Missimer, T. M., & Amy, G. L. (2013). Technical review and evaluation of the economics of water desalination: Current and future challenges for better water supply sustainability. Desalination, 309, 197–207. https://doi.org/10.1016/j.desal.2012.10.015

12 Global WASH Fast Facts | Global Water, Sanitation and Hygiene | Healthy Water | CDC. (2021, December 8). https://www.cdc.gov/healthywater/global/wash_statistics.html

13 Hu, J., Gupta, S. K., Ozdemir, J., & Beyzavi, M. H. (2020). Applications of Dynamic Covalent Chemistry Concept toward Tailored Covalent Organic Framework Nanomaterials: A Review. 31.

14 Jasechko, S., Perrone, D., Befus, K. M., Bayani Cardenas, M., Ferguson, G., Gleeson, T., Luijendijk, E., McDonnell, J. J., Taylor, R. G., Wada, Y., & Kirchner, J. W. (2017). Global aquifers dominated by fossil groundwaters but wells vulnerable to modern contamination. Nature Geoscience, 10(6), 425–429. https://doi.org/10.1038/ngeo2943

15 Kandambeth, S., Dey, K., & Banerjee, R. (2019). Covalent Organic Frameworks: Chemistry beyond the Structure. Journal of the American Chemical Society, 141(5), 1807–1822. https://doi.org/10.1021/jacs.8b10334

16 Kandambeth, S., Mallick, A., Lukose, B., Mane, M. V., Heine, T., & Banerjee, R. (2012).

Construction of Crystalline 2D Covalent Organic Frameworks with Remarkable Chemical (Acid/Base) Stability via a Combined Reversible and Irreversible Route. Journal of the American Chemical Society, 134(48), 19524–19527. https://doi.org/10.1021/ja308278w

17 Khan, N. A., Wu, H., Jinqiu, Y., Mengyuan, W., Yang, P., Long, M., Rahman, A. U., Ahmad, Nasir. M., Zhang, R., & Jiang, Z. (2021). Incorporating covalent organic framework nanosheets into polyamide membranes for efficient desalination. Separation and Purification Technology, 274, 119046. https://doi.org/10.1016/j.seppur.2021.119046

18 Khan, N. A., Yuan, J., Wu, H., Huang, T., You, X., Rahman, A. U., Azad, C. S., Olson, Mark. A., & Jiang, Z. (2020). Covalent Organic Framework Nanosheets as Reactive Fillers To Fabricate Free-Standing Polyamide Membranes for Efficient Desalination. ACS Applied Materials & Interfaces, 12(24), 27777–27785. https://doi.org/10.1021/acsami.0c06417

19 Kong, F., Yue, L., Yang, Z., Sun, G., & Chen, J. (2021). Cross-Linked Covalent Organic Framework-Based Membranes with Trimesoyl Chloride for Enhanced Desalination. ACS Applied Materials & Interfaces, 13(18), 21379–21389. https://doi.org/10.1021/acsami.1c03628

20 Li, C., Li, S., Zhang, J., Yang, C., Su, B., Han, L., & Gao, X. (2020). Emerging sandwich-like reverse osmosis membrane with interfacial assembled covalent organic frameworks interlayer for highly-efficient desalination. Journal of Membrane Science, 604, 118065. https://doi.org/10.1016/j.memsci.2020.118065

21 Li, X., Yang, C., Sun, B., Cai, S., Chen, Z., Lv, Y., Zhang, J., & Liu, Y. (2020). Expeditious synthesis of covalent organic frameworks: A review. Journal of Materials Chemistry A, 8(32), 16045–16060. https://doi.org/10.1039/D0TA05894G

22 Ni, L., Chen, K., Xie, J., Li, Q., Qi, J., Wang, C., Sun, X., & Li, J. (2022). Synchronizing formation of polyamide with covalent organic frameworks towards thin film nanocomposite membrane with enhanced nanofiltration performance. Journal of Membrane Science, 646, 120253.

https://doi.org/10.1016/j.memsci.2022.120253

23 Ohtani, E. (2020). The role of water in Earth's mantle. National Science Review, 7(1), 224–232. https://doi.org/10.1093/nsr/nwz071

24 Peng, L. E., Yang, Z., Long, L., Zhou, S., Guo, H., & Tang, C. Y. (2022). A critical review on porous substrates of TFC polyamide membranes: Mechanisms, membrane performances, and future perspectives. Journal of Membrane Science, 641, 119871. https://doi.org/10.1016/j.memsci.2021.119871

25 Pörtner, H.-O., & Roberts, D. C. (n.d.). Climate Change 2022: Impacts, Adaptation and Vulnerability. 3068.

26 Ritchie, H., & Roser, M. (2017). Water Use and Stress. Our World in Data. https://ourworldindata.org/water-use-stress

27 Rodell, M., Famiglietti, J. S., Wiese, D. N., Reager, J. T., Beaudoing, H. K., Landerer, F. W., & Lo, M.-H. (2018). Emerging trends in global freshwater availability. Nature, 557(7707), 651–659. https://doi.org/10.1038/s41586-018-0123-1

28 Shen, J., Yuan, J., Shi, B., You, X., Ding, R., Zhang, T., Zhang, Y., Deng, Y., Guan, J., Long, M., Zheng, Y., Zhang, R., Wu, H., & Jiang, Z. (2021). Homointerface covalent organic framework membranes for efficient desalination. Journal of Materials Chemistry A, 9(40), 23178–23187. https://doi.org/10.1039/D1TA06439H

29 Shi, X., Wang, R., Xiao, A., Jia, T., Sun, S.-P., & Wang, Y. (2018). Layer-by-Layer Synthesis of Covalent Organic Frameworks on Porous Substrates for Fast Molecular Separations. ACS Applied Nano Materials, 1(11), 6320–6326. https://doi.org/10.1021/acsanm.8b01537

30 Valentino, L., Matsumoto, M., Dichtel, W. R., & Mariñas, B. J. (2017). Development and Performance Characterization of a Polyimine Covalent Organic Framework Thin-Film Composite Nanofiltration Membrane. Environmental Science & Technology, 51(24), 14352–14359.

https://doi.org/10.1021/acs.est.7b04056

31 Wang, C., Li, Z., Chen, J., Li, Z., Yin, Y., Cao, L., Zhong, Y., & Wu, H. (2017). Covalent organic framework modified polyamide nanofiltration membrane with enhanced performance for desalination. Journal of Membrane Science, 523, 273–281. https://doi.org/10.1016/j.memsci.2016.09.055

32 Wang, H., Zhao, J., Li, Y., Cao, Y., Zhu, Z., Wang, M., Zhang, R., Pan, F., & Jiang, Z. (2022). Aqueous Two-Phase Interfacial Assembly of COF Membranes for Water Desalination. Nano-Micro Letters, 14(1), 216. https://doi.org/10.1007/s40820-022-00968-5

33 Wang, R., Shi, X., Xiao, A., Zhou, W., & Wang, Y. (2018). Interfacial polymerization of covalent organic frameworks (COFs) on polymeric substrates for molecular separations. Journal of Membrane Science, 566, 197–204. https://doi.org/10.1016/j.memsci.2018.08.044

34 Wang, R., Wei, M., & Wang, Y. (2020). Secondary growth of covalent organic frameworks (COFs) on porous substrates for fast desalination. Journal of Membrane Science, 604, 118090. https://doi.org/10.1016/j.memsci.2020.118090

35 Werber, J. R., Deshmukh, A., & Elimelech, M. (2016). The Critical Need for Increased Selectivity, Not Increased Water Permeability, for Desalination Membranes. Environmental Science & Technology Letters, 3(4), 112–120. https://doi.org/10.1021/acs.estlett.6b00050

36 Williams, J. (2022). Desalination in the 21st Century: A Critical Review of Trends and Debates. Water Alternatives, 15(2), 193–217.

37 Wu, Y., Wang, Y., Xu, F., Qu, K., Dai, L., Cao, H., Xia, Y., Lei, L., Huang, K., & Xu, Z. (2022). Solvent-induced interfacial polymerization enables highly crystalline covalent organic framework membranes. Journal of Membrane Science, 659, 120799. https://doi.org/10.1016/j.memsci.2022.120799

38 Xiao, A., Shi, X., Zhang, Z., Yin, C., Xiong, S., & Wang, Y. (2021). Secondary growth of bi-layered

covalent organic framework nanofilms with offset channels for desalination. Journal of Membrane Science, 624, 119122. https://doi.org/10.1016/j.memsci.2021.119122

39 Xiao, J., Chen, J., Liu, J., Ihara, H., & Qiu, H. (2022). Synthesis strategies of covalent organic frameworks: An overview from nonconventional heating methods and reaction media. Green Energy & Environment, S2468025722000796. https://doi.org/10.1016/j.gee.2022.05.003

40 Xu, L., Shan, B., Gao, C., & Xu, J. (2020). Multifunctional thin-film nanocomposite membranes comprising covalent organic nanosheets with high crystallinity for efficient reverse osmosis desalination. Journal of Membrane Science, 593, 117398. https://doi.org/10.1016/j.memsci.2019.117398

41 Yuan, J., Wu, M., Wu, H., Liu, Y., You, X., Zhang, R., Su, Y., Yang, H., Shen, J., & Jiang, Z. (2019). Covalent organic framework-modulated interfacial polymerization for ultrathin desalination membranes. Journal of Materials Chemistry A, 7(44), 25641–25649. https://doi.org/10.1039/C9TA08163A

42 Zhang, C., Wu, B.-H., Ma, M.-Q., Wang, Z., & Xu, Z.-K. (2019). Ultrathin metal/covalent–organic framework membranes towards ultimate separation. Chemical Society Reviews, 48(14), 3811–3841. https://doi.org/10.1039/C9CS00322C

43 Zhang, K., He, Z., Gupta, K. M., & Jiang, J. (2017). Computational design of 2D functional covalent–organic framework membranes for water desalination. Environmental Science: Water Research & Technology, 3(4), 735–743. https://doi.org/10.1039/C7EW00074J

44 Zhang, S., Zhao, S., Jing, X., Niu, Z., & Feng, X. (2021). Covalent organic framework-based membranes for liquid separation. Organic Chemistry Frontiers, 8(14), 3943–3967. https://doi.org/10.1039/D0QO01354D

45 Zhang, T., Li, P., Ding, S., & Wang, X. (2021). High permeability composite nanofiltration membrane assisted by introducing TpPa covalent organic frameworks interlayer with nanorods

for desalination and NaCl/dye separation. Separation and Purification Technology, 270, 118802. https://doi.org/10.1016/j.seppur.2021.118802

46 Zhou, W., Wei, M., Zhang, X., Xu, F., & Wang, Y. (2019). Fast Desalination by Multilayered Covalent Organic Framework (COF) Nanosheets. ACS Applied Materials & Interfaces, 11(18), 16847–16854. https://doi.org/10.1021/acsami.9b01883

Appendix: COFs Materials and Corresponding Monomers

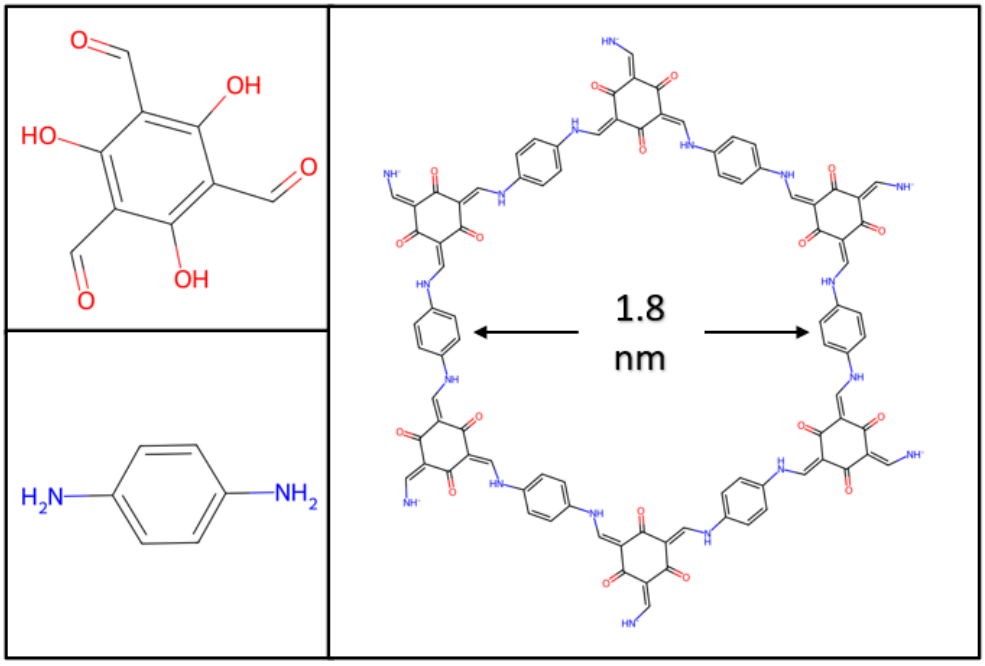

Figure A1. TpPa1 COF and corresponding monomers

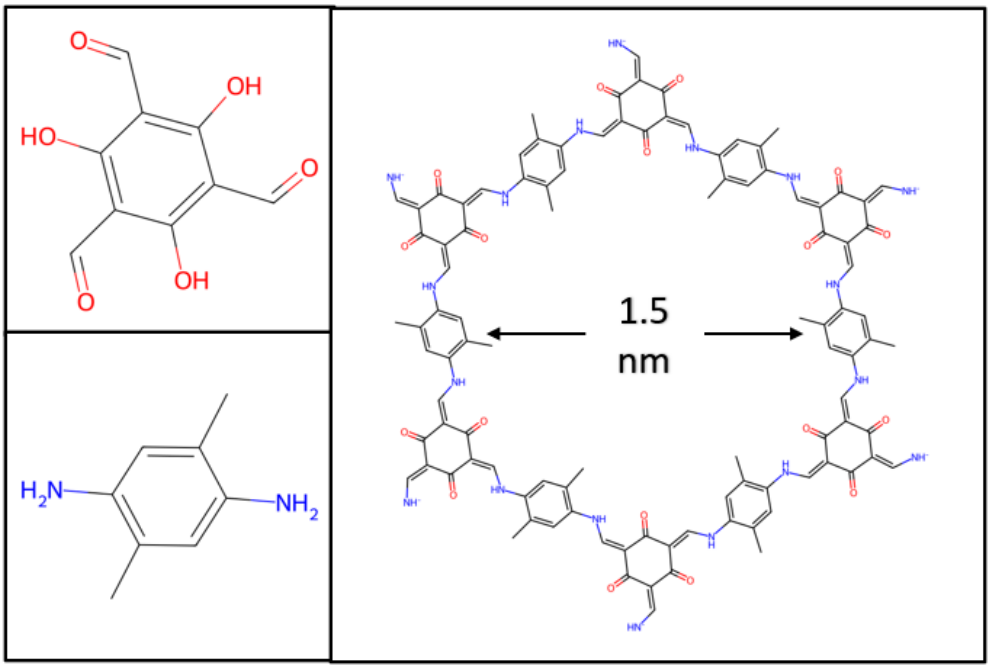

Figure A2. TpPa2 COF and corresponding monomers

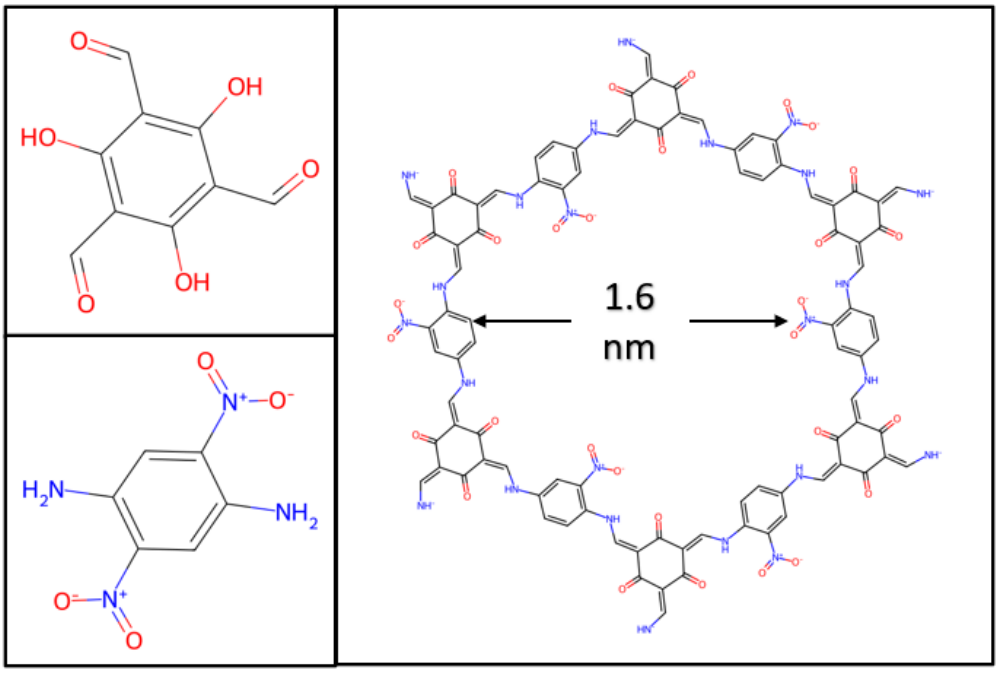

Figure A3. $TpPaNO_2$ COF and corresponding monomers

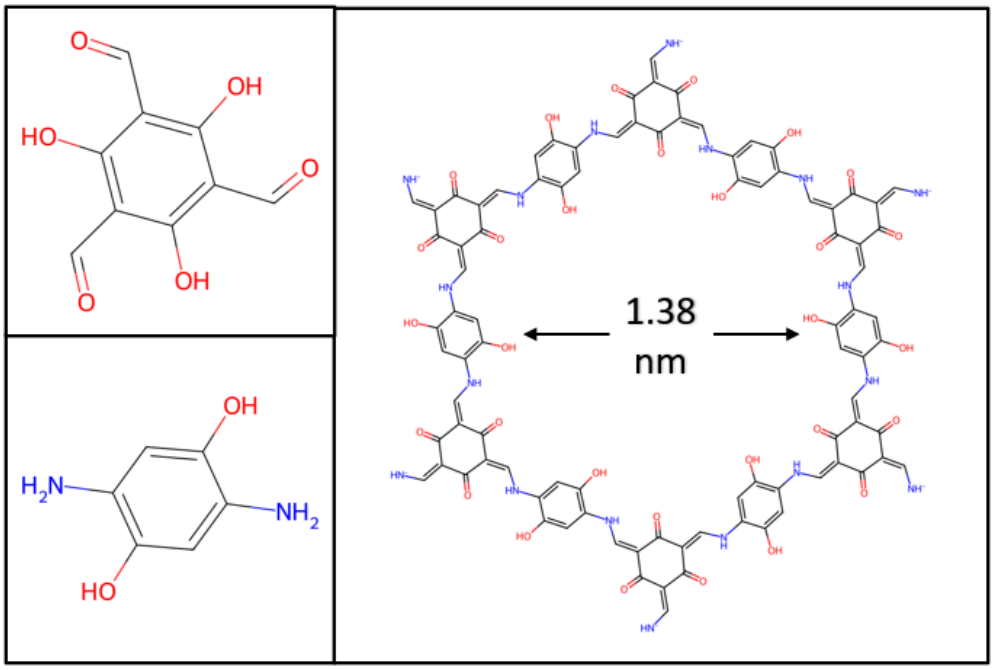

Figure A4. TpPa(OH)$_2$ COF and corresponding monomers

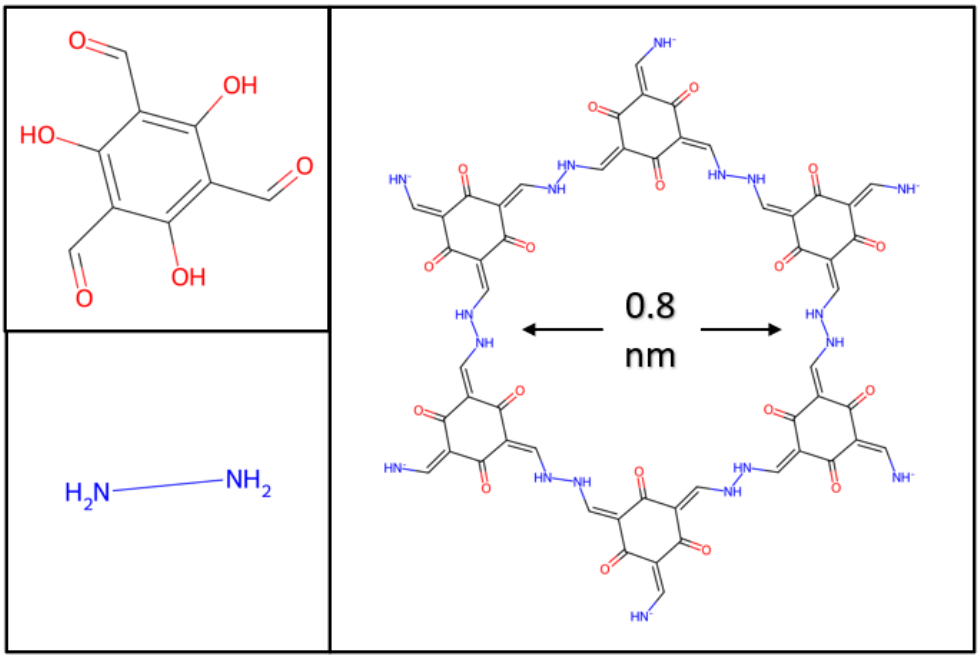

Figure A5. TpHz COF and corresponding monomers